Key Points:
- Burned areas produce substantially more surface runoff than unburned areas 3 years postfire even during extreme rainfall amounts
- Run-on into patchy high infiltration areas reduces simulated contributing areas to surface runoff 3 years after wildfire
- Connected near-channel low hydraulic conductivity areas produce most of the simulated surface runoff in the burned area

Correspondence to:
B. A. Ebel,
bebel@usgs.gov

Observed and simulated hydrologic response for a first-order catchment during extreme rainfall 3 years after wildfire disturbance

Brian A. Ebel[1], Francis K. Rengers[2], and Gregory E. Tucker[3]

[1]National Research Program, United States Geological Survey, Denver, Colorado, USA, [2]Geological Hazards Science Center, United States Geological Survey, Golden, Colorado, USA, [3]Department of Geological Sciences and Cooperative Institute for Research in Environmental Sciences, University of Colorado-Boulder, Boulder, Colorado, USA

Abstract Hydrologic response to extreme rainfall in disturbed landscapes is poorly understood because of the paucity of measurements. A unique opportunity presented itself when extreme rainfall in September 2013 fell on a headwater catchment (i.e., <1 ha) in Colorado, USA that had previously been burned by a wildfire in 2010. We compared measurements of soil-hydraulic properties, soil saturation from subsurface sensors, and estimated peak runoff during the extreme rainfall with numerical simulations of runoff generation and subsurface hydrologic response during this event. The simulations were used to explore differences in runoff generation between the wildfire-affected headwater catchment, a simulated unburned case, and for uniform versus spatially variable parameterizations of soil-hydraulic properties that affect infiltration and runoff generation in burned landscapes. Despite 3 years of elapsed time since the 2010 wildfire, observations and simulations pointed to substantial surface runoff generation in the wildfire-affected headwater catchment by the infiltration-excess mechanism while no surface runoff was generated in the unburned case. The surface runoff generation was the result of incomplete recovery of soil-hydraulic properties in the burned area, suggesting recovery takes longer than 3 years. Moreover, spatially variable soil-hydraulic property parameterizations produced longer duration but lower peak-flow infiltration-excess runoff, compared to uniform parameterization, which may have important hillslope sediment export and geomorphologic implications during long duration, extreme rainfall. The majority of the simulated surface runoff in the spatially variable cases came from connected near-channel contributing areas, which was a substantially smaller contributing area than the uniform simulations.

1. Introduction

1.1. Motivation

Extreme rainfall is increasingly recognized as a major driver of landscape response and evolution [e.g., *Korup and Clague*, 2009]. Extreme rainfall was defined herein as a 24 h rainfall with an exceedance probability less than or equal to 1/100. It impacts diverse processes including flood generation [e.g., *Ogden et al.*, 2000; *Smith et al.*, 2000, 2001, 2011], slope failure [*Borga et al.*, 2014], waterborne disease [*Curriero et al.*, 2001], dissolved organic carbon export [*Tittel et al.*, 2013], soil erosion [*Martínez-Casasnovas et al.*, 2002], and plant community dynamics [*Holmgren et al.*, 2006]. Rainfall ramifications are important in light of potential increases in observed and simulated rainfall intensity with global climate shifts [*Easterling et al.*, 2000; *New et al.*, 2001; *Kharin et al.*, 2007]. Landscape responses to extreme rainfall are further complicated by factors that affect rates and partitioning of water movement, such as landscape disturbance. Understanding disturbance hydrology [*Ebel and Mirus*, 2014] is critical in the western US because of increases in recent decades of landscape disturbances such as insect-driven vegetation mortality and wildfires [e.g., *Turner*, 2010]. Wildfire is one of the most important disturbances in the western US [e.g., *Turner et al.*, 1993; *Veblen et al.*, 1994; *Sherriff and Veblen*, 2006].

Predicting the effects of wildfire disturbance on hydrology requires knowledge of the affected processes as well as the magnitude and duration of disturbance impacts. Previous work has shown that wildfire can alter the hydrologic processes affecting runoff generation by influencing rainfall interception [e.g., *Stoof et al.*, 2012], surface roughness [e.g., *Stoof et al.*, 2015], soil sealing [e.g., *Neary et al.*, 1999; *Larsen et al.*, 2009],
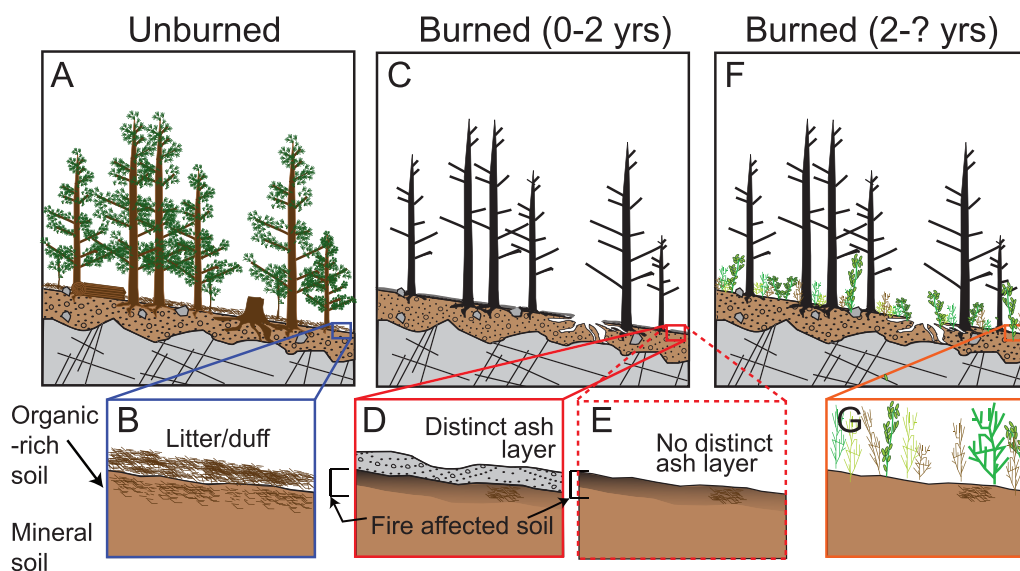
Figure 1. Conceptual schematic of the evolving wildfire effects on hillslope hydrology in the Colorado Front Range, USA. (A) Prewildfire state with closed or nearly closed canopy conifer forest. (B) Close-up of the near-surface soil, including a well-developed litter/duff layer and several cm of organic-rich soil. (C) Postwildfire state from immediately to a couple years after high-severity fire. Most of the vegetation canopy and fine fuels are combusted. (D) Close-up of the soil shows a distinct ash layer immediately after the fire and fire-affected soil. (E) Close-up of the soil illustrates the temporal transition to an indistinct ash layer after ash removal by water and wind action in addition to ash incorporation into the near-surface soil. (F) Landscape recovery from two years to decades after the wildfire disturbance. (G) Close-up of the soil showing understory vegetation regrowth and that fire effects on soils are recovering but may still be detectable.

litter/duff water storage [*Tiedemann et al.*, 1979; *Loaiciga et al.*, 2001], soil-water repellency [*Doerr et al.*, 2000; *MacDonald and Huffman*, 2004; *Jordán et al.*, 2011; *Mataix-Solera et al.*, 2013], soil-water retention [*Stoof et al.*, 2010; *Ebel*, 2012], soil-hydraulic properties controlling infiltration [*Robichaud*, 2000; *Martin and Moody*, 2001; *Moody et al.*, 2009; *Cerdà and Robichaud*, 2009], macropore flow [*Nyman et al.*, 2010, 2014], and water flow processes involving ash effects [*Cerdà and Doerr*, 2008; *Bodí et al.*, 2011, 2012; *Balfour and Woods*, 2013; *Balfour et al.*, 2014]. Collectively, these fire effects on hydrologic processes can result in major increases in runoff generation [*Shakesby and Doerr*, 2006; *Moody et al.*, 2013] and natural hazards including flash floods [e.g., *Moody and Martin*, 2001a] and debris flows [*Nyman et al.*, 2011; *Kean et al.*, 2011; *Staley et al.*, 2014], which motivates postdisturbance system characterization and modeling.

The typical temporal progression of wildfire effects at the hillslope scale in the Rocky Mountains of the US is generally known from prior studies in the region [e.g., *Morris and Moses*, 1987; *Moody and Martin*, 2001a, 2001b; *Benavides-Solorio and MacDonald*, 2001; *Larsen et al.*, 2009]. Before the wildfire, a dense forest (Figure 1A) with a well-developed litter/duff layer can be present, along with several centimeters of organic-rich soil underlain by rocky, mineral soil at depth (Figure 1B). Sparse forests are also present in the Rocky Mountains of the US, which may have thinner litter/duff layers than shown in Figures 1A and 1B. Hillslope runoff generation at the storm timescale for unburned landscapes in Figures 1A and 1B is almost exclusively controlled by subsurface stormflow in the Colorado Front Range because of high infiltration rates, rainfall interception, and surface cover [e.g., *Benavides-Solorio and MacDonald*, 2001]. After a high-severity wildfire, there is extensive combustion of the vegetation canopy and fine fuels, which reduces rainfall interception and exposes the soil surface (Figure 1C). Immediately following the fire, a distinct ash layer (Figure 1D) may be present. This ash layer will transition to a discontinuous or absent ash layer after ash removal by water and wind action in addition to incorporation into the near-surface soil (Figure 1E). The hillslope state shown in Figures 1C–1E often lasts for the first 2 years after high-severity wildfire in the Colorado Front Range. In recently disturbed, burned areas (Figures 1C–1E), infiltration-excess runoff is common [*Shakesby and Doerr*, 2006; *Kinner and Moody*, 2008; *Moody and Ebel*, 2014] because rainfall rates often exceed infiltration capacity (or infiltrability) [*Smith*, 2002], which can be reduced by the heat effects from wildfire [*Moody et al.*, 2013]. A few studies have observed saturation-excess runoff generation in wildfire-affected hillslopes generated at shallow depths (i.e., several cm) linked to reduced soil water storage from wildfire effects and ash layering

[*Onda et al.*, 2008; *Ebel et al.*, 2012]. As the landscape recovers from the wildfire disturbance, understory vegetation regrows (Figure 1F) and fire effects on soils are less obvious (Figure 1G) but may still be detectable.

Runoff generation mechanisms in landscapes in a partially recovered state are not well understood. Generation of runoff may occur by all hillslope mechanisms depending on initial conditions, rainfall intensities, and total storm amounts. There is a large body of postwildfire hydrologic research focused on the 1–2 year period after wildfires because this represents the time period with the greatest hydrologic change and accompanying natural hazards (e.g., flash floods and debris flows [e.g., *Prosser and Williams*, 1998; *Moody et al.*, 2013]). Recent work has recognized the importance of hydrologic disturbance effects over longer time periods as the landscape recovers (Figures 1F and 1G), vegetation regrows, and disturbance-driven process shifts are more subtle [*Inbar et al.*, 1998; *Cerdà and Doerr*, 2005; *Ubeda et al.*, 2005; *Wittenberg and Inbar*, 2009; *Tessler et al.*, 2013]. The total time for recovery of forest hydrologic function can range from as little as a few years [e.g., *Rowe et al.*, 1954; *Brown*, 1972; *Moody and Martin*, 2001a] up to decades [e.g., *Robichaud et al.*, 2000; *Shakesby and Doerr*, 2006] depending on fire conditions, climate, vegetation types, and soil factors.

Disturbed landscapes at various stages of wildfire recovery can be subjected to extreme rainfall, which motivates the need to predict the hydrologic response and associated natural hazards. Accurate predictions during extreme rainfall beyond previously observed magnitudes are challenging, because unexpected hydrologic processes may emerge as important and multiple runoff generation processes may become active [*Lyon et al.*, 2008]. This points to the need for (i) conceptual and hydrologic models without a priori assumptions regarding dominant hydrologic processes that lead to runoff generation and (ii) measurements and modeling efforts at well-characterized, disturbed sites subjected to extreme rainfall.

The primary motivation for this work was to address needs (i) and (ii), focusing on the coincidence of extreme rainfall and a landscape that has partially recovered (see Figures 1F and 1G) from wildfire disturbance 3 years prior to the extreme rainfall. Using numerical modeling together with data from the Colorado Front Range, USA, we sought the answer to the question of whether a previous wildfire disturbance matters during an extreme precipitation event or if, instead, the landscape generated surface runoff regardless of disturbance legacies.

The major objectives of this work were to:

1. Investigate the differences in measured soil-hydraulic properties between fire-affected and unburned soils.
2. Compare the peak surface runoff resulting from the extreme rainfall to measured peak surface runoff for similar rainfall intensities during the first 2 years after the wildfire. Peak surface runoff from the extreme rainfall was measured using indirect discharge estimation methods in the field. This analysis placed the peak surface runoff during the extreme rainfall event into a hydrologic-response magnitude context.
3. Simulate runoff generation during the extreme rainfall event and use numerical experiments to investigate (i) how partial recovery from the wildfire disturbance impacted hydrologic response and (ii) how spatial variability in soil-hydraulic properties affects infiltration, and thus runoff generation, following wildfire.

1.2. Research Area and Wildfire Disturbance

The 2010 Fourmile Canyon fire burned over 2300 hectares in the Front Range Foothills near Boulder, CO, USA in September 2010. Concerns over flooding motivated a multiyear study aimed at understanding hydrologic response to rainfall in burned and unburned areas in or adjacent to the 2010 Fourmile Canyon fire [*Moody and Ebel*, 2014; *Ebel et al.*, 2012; *Ebel*, 2012, 2013a, 2013b]. The primary research area for the previous work and the study reported here was a small first-order catchment at the western edge of the fire-affected area. This catchment (8440 m^2, Figure 2) lies on a ridge extending east from Sugarloaf Mountain, with an elevation range from 2350–2450 m, relatively steep slopes (15–28°), and predominately gravelly sand soils. Prior to the wildfire, the site was forested with primarily Douglas-fir (*Pseudotsuga menziesii* (Mirb.) Franco var. *glauca* (Beissn.)), Limber pine (*Pinus flexilis* James), and some aspen (*Populus tremuloides* Michx.) [*Moody and Ebel*, 2014; *Ebel*, 2012, 2013a, 2013b]. In this region of the Colorado Front Range, soils on north facing slopes, like those of the research area in this study, tend to develop thin O horizons, with variable or
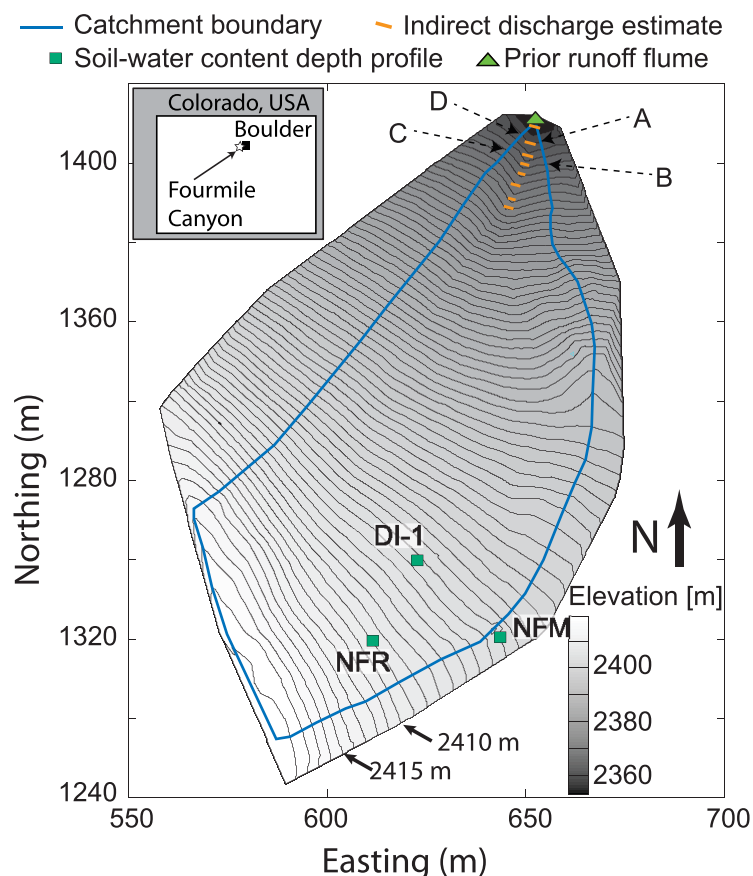
Figure 2. Map of the research area near Sugarloaf upstream of Boulder, CO, USA affected by both the 2010 Fourmile Canyon Fire and the September 2013 extreme rainfall. Burned location names are north facing ridge (NFR), north facing midslope (NFM), and difference infiltrometer 1 (DI-1). Points ABCD mark points of surface boundary condition specification in the hydrologic response model. Topographic contours are every 1 m.

absent E horizons, and thicker B and C horizons that are classified as Cryalfs or Ustalfs [*Birkeland et al.*, 2003]. Underlying bedrock at the research site is predominantly Boulder Creek Granodiorite [*Gable*, 1980].

1.3. The September 2013 Extreme Rainfall Event

Historically unprecedented rainfall from the September 2013 storms along the Front Range Mountains in Colorado, USA provided a test of how extreme rainfall might change the hydrologic response in a landscape with spatially variable hydrologic disturbance caused by wildfire. The hydrometeorology of this extended storm was detailed in *Gochis et al.* [2015] and briefly summarized here. Steady accumulating rain fell from 10 to 16 September with embedded cells of higher rainfall intensity [*Lucas*, 2013; *Gochis et al.*, 2015]. This rainfall was concentrated in a relatively narrow (∼40 km wide × ∼200 km long) band-trending SSE-NNW from Boulder to Estes Park, Colorado across the predominantly west-east drainage system of the Front Range Mountains [*HDSC*, 2013; *Moody*, 2016]. Rainfall totals from 9–16 September in excess of 250 mm were widespread, with the greatest amounts, exceeding 400 mm, in the vicinity of Boulder and in the foothills to the west and northwest [*Gochis et al.*, 2015]. A new 24 h rainfall record was set in the city of Boulder [*Coe et al.*, 2014] for a rain gage dating from 1893 [*Perica et al.*, 2013].

2. Experimental Methods

2.1. Rainfall

Rainfall during the September 2013 storms was recorded by nearby tipping-bucket rain gages operated by the Urban Drainage and Flood Control District (www.Udfcd.org) which telemetered the time of each tip. The closest gage to the study site (Sugarloaf, ID number 4730) was 1.5 km from the research area. Cumulative rainfall from the Sugarloaf gage was converted into 5, 10, and 30 min average rainfall rates. There was considerable variability at the regional scale of total rainfall and rainfall rates during the September 2013 storms [*Gochis et al.*, 2015]. Total rainfall contours shown in *Coe et al.* [2014] suggested that at the scale of the research area (<1 ha), using the nearest rain gage provides adequate spatial characterization.

2.2. Soil Depth

Soil depth is a first-order control on soil-water storage and the geometry of the soil-bedrock interface can affect subsurface flow. Soil depth was measured in the research area using a steel rod driven to refusal because the intention was to characterize the soil interface with the weathered bedrock. Three to four repeat soil-depth measurements were taken at each location and the deepest value was used to reduce the

bias caused by the presence of large stones in the soil profile. A total of 91 locations of soil depth, with three to four measurements per location, were measured in the study area.

2.3. Soil-Hydraulic Properties

Soil-hydraulic property and water repellency data indicate rates of water entry into the soil and the propensity for infiltration-excess runoff relative to observed rainfall rates. Two key properties measured are field-saturated hydraulic conductivity, K_f, and sorptivity, S. S dominates behavior in the early period of infiltration (<30 min for sandy soils [*White and Sully*, 1987]), while K_f dominates behavior in later periods (hours); the long multiday duration of the September 2013 storms suggested that K_f was likely to be the more important control on infiltration and thus runoff generation. Water movement from the soil into the weathered bedrock system is also controlled by K_f and S. The properties K_f and S were estimated using a mini-disc infiltrometer [*Decagon Devices*, 2006] at 1 cm of tension. Mini-disc infiltrometers have been used successfully to characterize infiltration rates in a variety of soils, including those affected by wildfire [*Lewis et al.*, 2006; *Moody et al.*, 2009; *Moody et al.*, 2016]. Soil surface measurements were conducted from 7–20 November 2013, approximately 2 months after the flooding when site access was restored. Soil surface infiltration measurements were made in the burned research area (N = 14) near the NFR, NFM, and DI-1 locations (Figure 2) and in the nearby unburned area (N = 11) by the UBNF location (approximately 500 m away, see location in *Ebel* [2013a, 2013b]). Weathered bedrock infiltration measurements (N = 4) were made in the burned area near the DI-1 location in the summer of 2014 by excavating a trench to the soil interface (55–60 cm below land surface) with the weathered bedrock and preparing a small, planar surface for the mini-disc infiltrometer placement using a sharpened putty knife. To ensure one-dimensional flow (i.e., vertical), a 4.4 cm diameter metal ring was driven into the porous media prior to measurement and a small plastic collar was used to seal this ring to the infiltrometer. Litter and duff were removed from the surface prior to the unburned soil measurements to ensure good infiltrometer contact with the soil. Litter and duff removal assumed that the litter and duff were not limiting infiltration in the unburned area, which was supported by constant head permeameter tests (method in *Reynolds and Elrick* [2002]) of saturated hydraulic conductivity on repacked litter/duff samples where K_f was 1760 mm h^{-1} [*Ebel*, 2013b]. Litter and duff were not present atop the soil in the burned area where infiltration measurements were collected. For the weathered bedrock infiltration measurements, a thin layer of sand sieved from the field area was used to ensure good contact between the infiltrometer base and the soil surface [see *Reynolds and Zebchuk*, 1996].

The cumulative infiltration into the soil, I [mm], was estimated using a one-dimensional (i.e., vertical) equation [*Vandervaere et al.*, 2000]

$$I = S\ t^{0.5} + [(2-\beta)/3]K_f\ t,$$ (1)

where S is sorptivity [mm h$^{-0.5}$], t is time [h], β is an integral shape parameter assumed to be 0.6 [*Vandervaere et al.*, 2000], and K_f is the hydraulic conductivity [mm h^{-1}] at the final soil-water content. Infiltration measurements were fit with nonlinear least squares minimization using the Trust-Region method [*Moré and Sorensen*, 1983] in the software MATLAB (https://www.mathworks.com/products/matlab/), which allowed the constraint that S and K_f be greater than zero. Statistical tests to provide strength of evidence used the Wilcoxon rank sum test performed in the software MATLAB. The *p*-value was calculated using the exact method because of the relatively small sample sizes. The null hypothesis was that the values of the soil-hydraulic property of interest in the burned and unburned sites were from continuous distributions with equal medians. Water drop penetration times, a measure of soil-water repellency persistence, were measured and classified (N = 21 for burned and N = 18 for unburned sites) adjacent to the infiltration rate measurements using the method of *Dekker et al.* [2009]. Because soil-water repellency and S depend on soil-water content, soil-water content measurements for 0–3 cm depth were collected using a 4.7 cm diameter corer (four replicates for burned soils and four replicates for unburned soils near the soil-water repellency data). Soil-water content samples were processed using the thermogravimetric method [*Topp and Ferré*, 2002].

2.4. Soil-Water Content and Saturation

Volumetric soil-water content, θ [cm^3 cm^{-3}] was measured during the September 2013 storms at three locations (NFR, NFM, and DI-1, Figure 2) at depths of 5, 10, 15, 20, 25, and 30 cm within the burned research area and one companion unburned location (UBNF) on a nearby north-face slope approximately 500 m

away. Soil-water content measurements at several depths were made using automated subsurface sensors (Decagon 5TE, Decagon Devices), sampled at 5 min temporal resolution. These sensors were previously calibrated for the soil from each location [*Cobos and Chambers*, 2010] and temperature corrected [*Cobos and Campbell*, 2007] with accuracy to ± 0.01 to 0.02 cm^3 cm^{-3}. Volumetric soil-water content was converted to saturation by dividing by saturated soil-water content measured at each location [*Ebel*, 2012].

2.5. Peak Surface Runoff

Indirect measurements of peak surface runoff were made within the main channel of the burned area (see Figure 2) following the September 2013 floods because the 3 inch modified Parshall [*Ebel et al.*, 2012] flume at the catchment outlet had been removed in 2012. Indirect estimation of peak surface runoff relied on two steps. The first step was measuring channel cross-sectional area between high-water marks (identified on 22 September 2013 and resurveyed on 2 June 2015) following the September 2013 rain storms. The second step computed estimates of flow velocity using multiple methods [*Moody*, 2016]. Elevation of channel cross sections were measured using a metric rod and survey level (NAK2, Wild Heerbrugg Instument) at 5 cm spacing across each of eight cross sections (see Figure 2). A longitudinal profile of the channel was also surveyed at 5 cm spacing to determine a roughness metric equal to the standard deviation of the bed elevation, σ_z, uphill from each cross section. Additionally, the protrusion height of 129 roughness elements were measured on a grid (0.3 m cross channel $\times$ 0.5 m along channel and covering 22 m of channel) to determine the roughness metric, D_{84} (diameter for which 84% of elements are smaller).

Four different methods were used to calculate an ensemble average of peak surface runoff and its uncertainty ($\pm$one standard deviation) [*Moody*, 2016]. The methods were (1) average values of Manning's "n" (0.21 ± 0.07 s m$^{-1/3}$) measured in 2011 at multiple sites in hillslope drainages on the upper part of the study area, (2) an empirical resistance equation for step-pool mountain stream [*Yochum et al.*, 2012, model 17, Table 6, reach slopes 0.07–0.21], (3) an empirical resistance equation for high-gradient streams [*Comiti et al.*, 2007, Figure 7, reach slopes 0.02–0.19] where D$_{84}$ was estimated as two times σ_z, and (4) the critical flow method [*Yochum and Moore*, 2013].

2.6. Hydrologic Response Model

The numerical model used in this study to simulate hydrologic response was the Integrated Hydrology Model (InHM) [*VanderKwaak*, 1999], which was developed at the University of Waterloo. The model simulated unsaturated subsurface flow in three-dimensions (3-D) and surface/channel flow in two dimensions (2-D) using the control-volume finite-element method with a fully coupled approach. Variably saturated subsurface flow through porous media was simulated using Richards equation. The diffusion-wave approximation to the depth-integrated shallow water equations was used to simulate surface water flow. A fully coupled approach using first-order exchange coefficients linked the surface and subsurface continua [*VanderKwaak*, 1999; *Ebel et al.*, 2009]. Surface water velocities were given by the 2-D Manning water depth/friction discharge equation. InHM has been used at a large range of temporal and spatial scales from plot and catchment [*BeVille et al.*, 2010; *Loague et al.*, 2010; *Ran et al.*, 2007] to watershed scales [e.g., *Smerdon et al.*, 2007; *Jones et al.*, 2008; *Heppner and Loague*, 2008; *Carr et al.*, 2014; *Ran et al.*, 2012] and across the full spectrum of runoff generation mechanisms [*Mirus et al.*, 2011; *Mirus and Loague*, 2013].

2.7. Hydrologic Model Boundary Conditions, Initial Conditions, and Parameterization

The hydrologic response model required boundary and initial conditions as well as parameterization of properties within the domain. The finite-element mesh for the research catchment consisted of 2668 surface nodes and 117,392 subsurface nodes. The mesh discretization was spatially variable, with vertical discretization (Δz) from 0.01 to 0.08 m (near-surface soil) to 0.33 m (weathered bedrock) and lateral discretizations (Δx, Δy) from 0.2 to 3.3 m. Topography was based upon a 2333 point total station survey. An adaptive time step (Δt) was used that adjusts relative to mass conservation and time derivative criteria of state variables in the surface and subsurface resulting in time steps $\ll 1$ s to 1 h. Surface boundary conditions were a specified flux to represent precipitation (evaporation and transpiration are omitted), a critical depth [*Chow*, 1959] at the downgradient surface flow boundary (line AD in Figure 2), and no flow at the surface boundaries not represented by a critical depth. The subsurface boundary conditions were an upstream-weighted, implicitly calculated flux [*VanderKwaak*, 1999; *Mirus et al.*, 2011] across the downgradient face (below CDAB in Figure 2) as well as the basal (i.e., bottom of the weathered bedrock) boundary

Table 1. Hydrogeologic Properties Used in Hydrologic Response Model Parameterization[a]

Layer	$\theta_S{}^b$ (cm^3 cm^{-3})	$\theta_r{}^b$ (cm^3 cm^{-3})	α^b (m^{-1})	N^b	K_s or K_f (mm h^{-1})
Burned soil (0–3 cm)	0.49	0.008	3.97	1.401	5.6 or variable[c]
Burned soil (3 cm to base)	0.49	0.008	3.97	1.401	432[d]
Weathered bedrock	0.098	0.01	7.05	1.446	63.7[c]
Unburned soil (0–3 cm)	0.46	0.01	7.05	1.446	279 or variable[c]
Unburned soil (3 cm to base)	0.46	0.01	7.05	1.446	185[d]

[a]Hydraulic conductivity as a function of saturation is represented using the *Mualem* [1976] approach based on the *van Genuchten* [1980] parameters.
[b]*van Genuchten* [1980] parameters for soil-water retention; θ_s is the saturated soil-water content, θ_r is the residual soil-water content, α and n are the two soil-water retention curve fitting parameters.
[c]Minidisc tension infiltrometer measurement.
[d]Constant head permeameter measurement in laboratory [*Ebel*, 2013b]; burned soil *van Genuchten* [1980] parameters are based on the NFR location measurements reported in *Ebel* [2012]; unburned soil *van Genuchten* [1980] parameters are based on the UBNF location measurements reported in *Ebel* [2012].

and impermeable at the upgradient and lateral boundaries. The surface coupling length scale was set to 10^{-5} m to tightly couple the surface and subsurface continua [*Ebel et al.*, 2009; *Liggett et al.*, 2012].

The hydrologic-response model required representation of soil and geologic layering/geometry and soil-water retention relationships. The soil layer depth was based on field measured soil depths that were interpolated across the field site using ordinary kriging in the software Surfer (http://www.goldensoftware.com/products/surfer) and incorporated into the subsurface finite-element mesh. Geologic layering depths were the same between burned and unburned simulations. A 3 cm thick surficial soil layer represented the depth characterized by the tension infiltrometer measurements reported here. Independent of these measurements, this 3 cm thick soil layer was also observed in field characterization and soil-water content observations [*Ebel*, 2013a], and its existence was supported by numerical simulation of observed soil-water content data from that depth [*Ebel*, 2013b]. The thickness of the remaining soil was spatially variable based on the kriged soil depths. Weathered bedrock thickness was set to a constant value of 10 m, which was iteratively increased to ensure that it had minimal effects on simulated flow from the soil into the weathered bedrock. The soil-water retention relations [*van Genuchten*, 1980] were based on laboratory characterization at the site [*Ebel*, 2012] and prior one-dimensional (vertical) simulation-based work [*Ebel*, 2013b]. The van Genuchten relations were fit, using the software RETC [*van Genuchten et al.*, 1991], to measured soil-water retention data from intact soil cores taken from the near-surface (1–8 cm depth) at the site [*Ebel*, 2012]. Porosity was also estimated using the saturated soil-water content (θ_S) from the soil-water retention measurements. The weathered bedrock θ_S value and soil-water retention relationships for the weathered bedrock were not known for this site. In the absence of other information, the weathered bedrock van Genuchten parameters were set to the unburned north facing soil values estimated for the site [*Ebel*, 2012; *Ebel*, 2013b] and the θ_S value was set to the saprock value of porosity (0.098) based on bulk density values (assuming solid density of 2.65 g cm^{-3}) from *Parizek and Girty* [2014] for Sugarloaf Mountain, which was adjacent to this research area. Porous media compressibility for all layers was set to 1×10^{-8} m s^2 kg^{-1} [*Freeze and Cherry*, 1979]. The porous media parameterization is summarized in Table 1. Manning's roughness for the burned hillslope was set to 0.21 s m$^{-1/3}$ based on hillslope velocity measurements conducted in September 2011; the measured values ranged from 0.13 to 0.29 s m$^{-1/3}$. These measurements were for estimated relatively shallow flow depths of ~0.005 m. For deeper depths the value of Manning's roughness would be less. Model sensitivity to roughness was examined using the range of measured values from 0.13 to 0.29 s m$^{-1/3}$. Manning's roughness for the hillslope was assumed to be isotropic.

Initial conditions were estimated using the measured soil-water content profiles in the soil. The soil-water content profiles were nearly uniform between 5 and 30 cm on 9 September 2013 at midnight, with a mean saturation value of 0.139 ± 0.01 within the burned research area and saturation of 0.146 ± 0.02 at the nearby unburned location. The ± denotes one standard deviation of the saturation calculated from soil-water content measurements for the entire 5–30 cm profile at the time of the initial condition. Model initial conditions were set in terms of pressure head using the van Genuchten relations. In the absence of information regarding the θ of the weathered bedrock, the initial condition in this layer was set to be the same pressure head as the value for the soil (note this is a different θ because of the different θ_S). The initial surface water
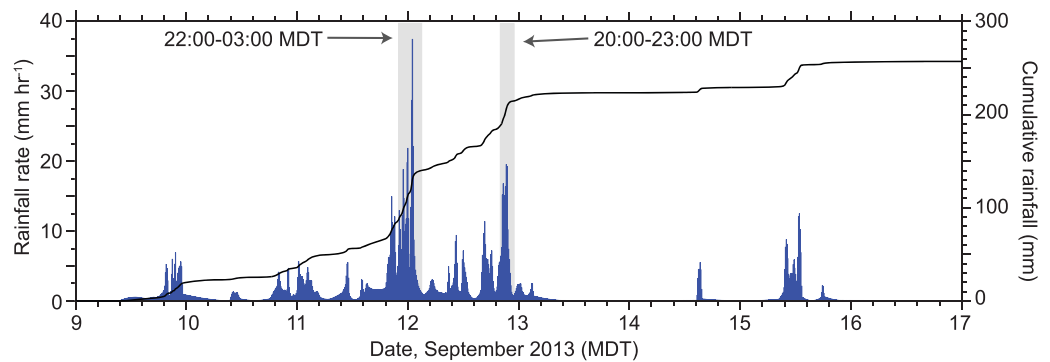
Figure 3. Time series of rainfall during the 2013 storms at 10 min intensity from the Sugarloaf rain gage (ID number 4730) operated by the Urban Drainage and Flood Control District (www.Udfcd.org). The Sugarloaf gage is 1.5 km from the research area.

depth was set to a very small value, 1×10^{-5} m, at all surface nodes for numerical stability during initial solution time steps.

The minidisc infiltration measurements were used to parameterize K_f in the hydrologic response model for 0–3 cm depth, which was the depth of the metal ring used to ensure 1-D vertical flow and the assumed approximate support depth. Constant-head permeameter measurements in the laboratory were used to parameterize soil properties in a layer extending from 3 cm depth to the base of the soil. K_f was treated as homogeneous and isotropic within a given model layer (except for the 0–3 cm depth). The 0–3 cm depth values for K_f were specified using two methods. The first was an effective hydraulic conductivity approach that used the geometric mean of the measured K_f values from the minidisc estimates. The second approach for representing K_f values specified spatially variable values by random sampling from the measured K_f with no specification of spatial correlation. 100 realizations of K_f were used to examine controls on simulated run-off. Individual realizations were generated by random sampling with replacement from the measured K_f values (i.e., simple or naïve bootstrap [*Efron*, 1979]) assigned to the finite-element nodes grouped vertically, representing the soil column from 0 to 3 cm depth. This method created two-dimensional (lateral) spatial variability but not vertical spatial variability within the top 3 cm of soil.

3. Results and Discussion

3.1. Rainfall

Rainfall rates were used to interpret the propensity for infiltration-excess runoff generation, when compared to soil-hydraulic property magnitudes, and to parameterize the surface boundary condition in the numerical model. The measured rainfall intensities differed little between 5 and 10 min durations, but were appreciably less at times of peak intensities for 30 min durations. The maximum intensity for 5 min was 41.2 mm h^{-1}, for 10 min was 40.2 mm h^{-1}, whereas for 30 min rainfall it was 30.7 mm h^{-1}. Because the 10 min data tended to be less noisy than the 5 min data and still captured the magnitude of shorter bursts of high intensity rainfall that may drive infiltration-excess runoff generation, the 10 min data were used as the rainfall input into the hydrologic model (Figure 3). Rainfall rates during the September 2013 storms were moderate to low intensity with two periods of higher sustained rates from 22:00 to 3:00 MDT, 11–12 September and from 20:00 to 23:00 on 12 September (highlighted in Figure 3 with shaded boxes). These higher rainfall periods served as the focal point for simulated surface runoff generation examined here.

3.2. Soil Depth

Soil depths in the research area were relatively shallow, becoming deeper along the hollow axis relative to the interfluves and uppermost topographic divide. There was a relatively narrow range in soil depths (Figure 4A). The mean soil depth was 0.39 m, the maximum was 0.83 m, the minimum is 0.1 m, and the standard deviation was 0.12 m (N = 91). The variability in soil depth is shown by the box plot in Figure 4A. This shows the relatively narrow range in soil depths, with the first quartile equal to 0.31 m and the third quartile equal to 0.44 m (i.e., interquartile range of 0.13 m, Figure 4A). Soil depth appeared reasonably approximated by a normal distribution (Figure 4B) but was not normally distributed based on Kolmogorov-Smirnov and
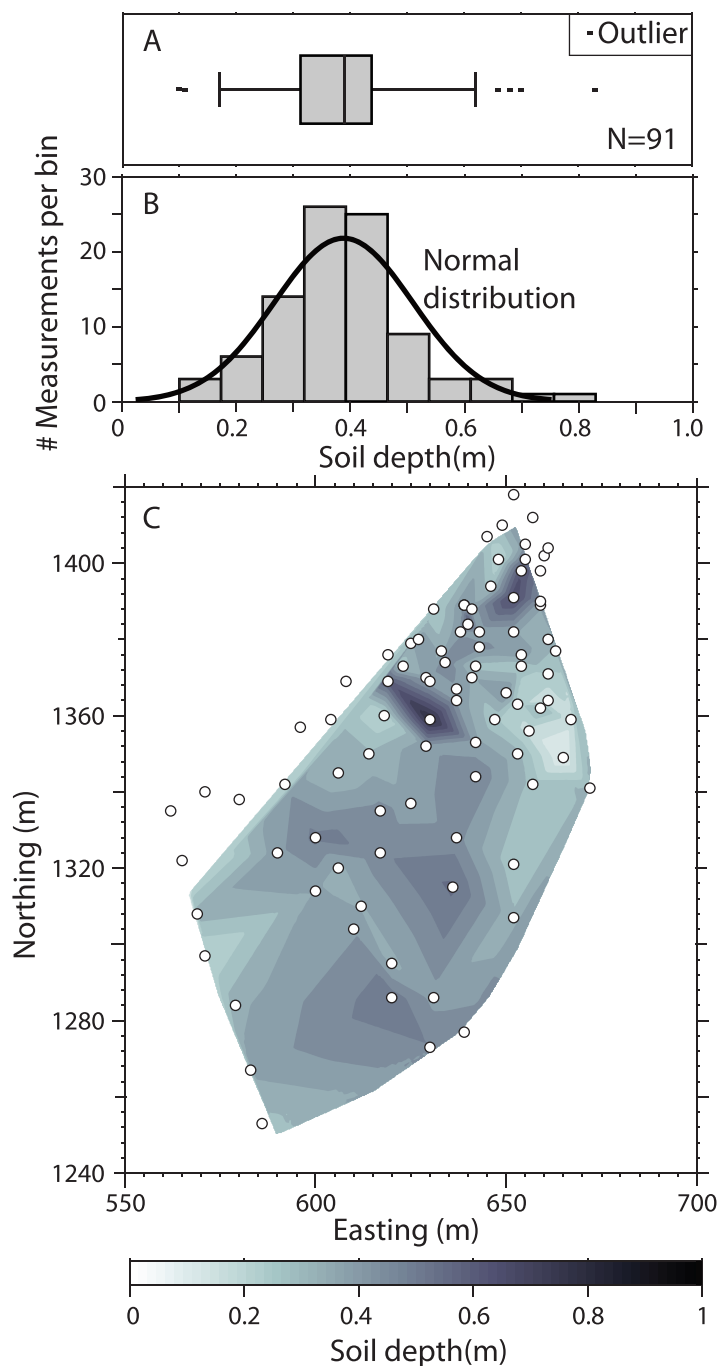
Figure 4. Characterization of soil depth at the research area. (A) Box and whiskers plot of soil depth measurements. First and third quartile are 0.31 and 0.44 m, respectively. (B) Histogram of soil depth measurements and fit for a normal distribution. (C) Interpolated map of soil depth and overlain measurement locations (white circles). Interpolation is conducted using ordinary kriging and an omnidirectional variogram in the software Surfer.

Lilliefors statistical tests in the software MATLAB ($\alpha = 0.05$). Kriged soil depths (Figure 4C) were greater in the hollow axis and shallower at the catchment margins, as expected.

3.3. Soil-Hydraulic Properties

Soil-hydraulic property measurements showed that there was greater variability in the burned area with some areas of the burned hillslope that were essentially impermeable. Surface soils in the burned area had lower K_f and lower S than surface soils in the unburned area based on geometric and arithmetic means, respectively (Table 2 and Figure 5). Variability in K_f was larger in the burned area and variability in S was larger in the unburned area based on interquartile ranges and standard deviations. The statistical test provided no evidence against the null hypothesis for the S data (p-value = 0.935), suggesting there was little difference between the S values at the burned and unburned sites. By contrast, the statistical test provided moderate evidence against the null hypothesis for the K_f data (p-value = 0.011), suggesting there was likely a difference in K_f between burned and unburned soils. Because soil-water content was elevated by the long-duration rainfall from 9 to 12 September, the effect of S on infiltration and runoff generation was assumed to be minor relative to K_f. Previous measurements of K_f in 2010 at the research area were 10 mm h^{-1} on a severely burned north facing hillslope and 720 mm h^{-1} on an unburned north facing hillslope, both arithmetic means [*Ebel et al.,*

2012]. The burned soils in 2010 had more measurements of K_f that were nearly impermeable for the 30 min measurement duration (8 out of 12 measurements, median K_f was zero [*Ebel et al.*, 2012]) compared to 2013 when only two measurements had very small K_f values. One-dimensional (vertical) modeling estimates for the summer of 2011 had a best fit value of K_f equal to 5.2 mm h^{-1} on enclosed runoff plots on the burned north facing hillslope [*Moody and Ebel*, 2014]. Numerous studies in the Colorado Front Range have shown decreases in infiltration

Table 2. Soil-Hydraulic Properties of Hydraulic Conductivity, K_f, and Sorptivity, S, Estimated Using a Minidisc Infiltrometer [*Decagon Devices*, 2006] at 1 cm of Tension[a]

| | N | K_f (mm h^{-1}) | | | | S (mm h$^{-0.5}$) |
		Mean_{Geom}	Median	Maximum	Minimum	Mean_{Arith}
Unburned soil	11	279 ± 138	373 ± 138	487	81.9	16.1 ± 19.3
Burned soil	14	5.6 ± 188	77.8 ± 188	628	∼0	11.8 ± 9
Weathered bedrock	4	63.7 ± 47.5	100.3 ± 47.5	116.4	14.2	13.1 ± 6.1

[a]Mean_{Geom} is the geometric mean; Mean_{Arith} is the arithmetic mean; ± is 1 standard deviation. The two very small K_f values were included as the values produced by the nonlinear least squares fitting (i.e., not zero) in the calculation of the geometric mean and in the spatially variable K_f simulations.

rates lasting 1–2 years after wildfire [e.g., *Robichaud*, 2000; *Martin and Moody*, 2001; *Kinner and Moody*, 2008, 2010; *Larsen et al.*, 2009]. Far less research has been devoted to longer-term (i.e., 2–10 years) recovery of infiltration rates after wildfire. A study by *Cerdà* [1998] reported that for Mediterranean scrubland 6 years elapsed after the fire before infiltration rates returned to unburned levels. The measured K_f values here indicated moderate evidence (p-value = 0.011) in support of differences between burned and unburned hillslopes 3 years after wildfire, suggesting that the recovery of K_f in this area can take over 3 years following high severity wildfire.

The differences in K_f and the magnitude of the measured K_f values have important implications for runoff generation. For example, the geometric mean of the burned area-values was below the apparent 30 min rainfall rate threshold (10 mm h^{-1}) for postwildfire infiltration-excess runoff [*Moody and Martin*, 2001a, 2001b; *Kunze and Stednick*, 2006]. In the context of the rainfall rates during the September 2013 storms, the maximum 10 min rainfall rate lay between the first and second quartile of the burned hillslope K_f values (Figure 5A), suggesting infiltration-excess runoff generation from some low K_f areas. By contrast, the maximum 10 min rainfall rate lay considerably below the lower limit of the unburned K_f values (Figure 5A) suggesting no infiltration-excess runoff was generated on soil in unburned hillslopes.

Water repellency metrics indicated that most areas of the burned hillslope showed only slight water repellency although a few areas were still strongly water repellent despite 3 years of elapsed time since the wildfire. Soils in the burned area (N = 21) had water-drop penetration times between 1 and 30 s (slightly water repellent [*Dekker et al.*, 2009] with the exception of the two measurements where K_f values were
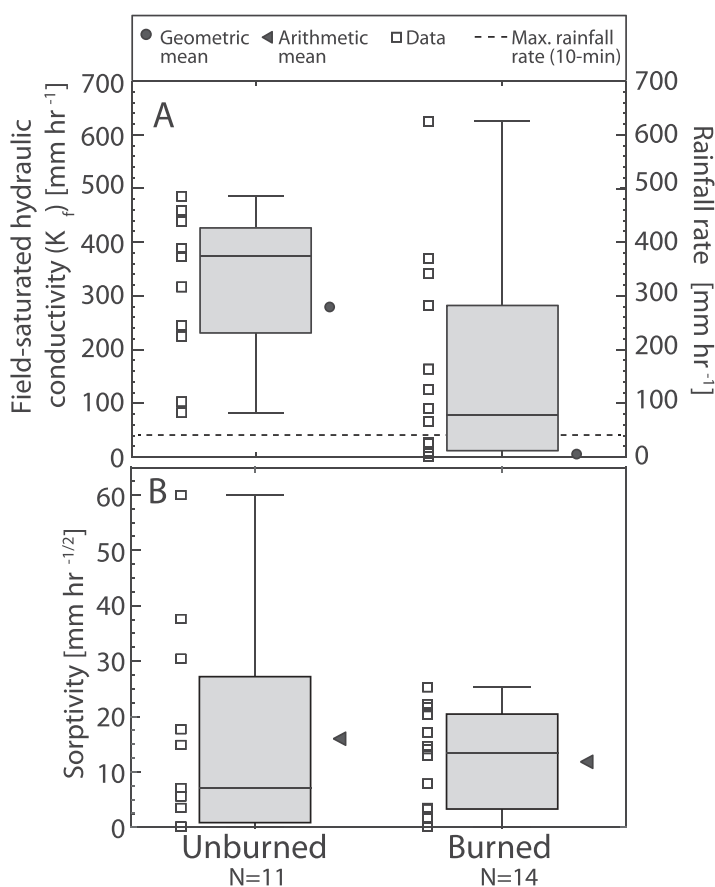
Figure 5. Box and whiskers plots of soil-hydraulic properties determined from tension infiltrometer data from burned and unburned areas. The middle line within the box is the median, the edges of the box denote the 25th and 75th percentiles, the whiskers mark data extent of the nonoutliers, and the small boxes show the distribution of data values used to construct the box plots. (A) Hydraulic conductivity and the overlain line denoting maximum observed 10 min rainfall intensity. (B) Sorptivity.

very small values and water drop penetration times were 5 min or more (strongly water repellent [*Dekker et al.*, 2009]). By contrast, soils in the unburned area had water drop penetration (N = 18) times of only a few seconds (nonwater repellent [*Dekker et al.*, 2009]). The associated mean soil-water content in the top 3 cm of soil at the time of soil-hydraulic property and repellency measurement (approximately 2 months after extreme rainfall event) was 0.084 ± 0.023 cm^3 cm^{-3} (N = 4) in the burned area and 0.183 ± 0.034 cm^3 cm^{-3} (N = 4) in the unburned area. Water repellency depends on soil-water content and *Doerr and Thomas* [2000] and *Huffman et al.* [2001] showed that at higher soil-water contents soil-water repellency can decrease substantially, and this may in turn reduce runoff [*Benavides-Solorio and MacDonald*, 2001]. The unburned soil-water content during water-drop penetration time measurements was above an effective repellency threshold value of 0.1 cm^3 cm^{-3} for unburned soils [*MacDonald and Huffman*, 2004] but below an effective repellency threshold value for high-severity burned soils of 0.26 cm^3 cm^{-3} [*MacDonald and Huffman*, 2004]. The soil-water content of the soils at the time of sampling may affect the water drop penetration times, but nonetheless suggested fire-enhanced soil-water repellency in some areas of the burned catchment. These measurements of infiltration and soil-water repellency were not spatially comprehensive enough to make definitive conclusions regarding runoff generation, but the measurements facilitated the development of further insight through numerical experiments with the hydrologic response model.

3.4. Indirect Discharge Estimates

The indirect peak surface runoff estimate during the September 2013 storms facilitated comparison to measured peak surface runoff in the research area immediately after the wildfire when infiltration-excess runoff dominated [*Moody and Ebel*, 2014]. The indirect estimated peak surface runoff during the September 2013 storm ranged from 0.038 m^3 s^{-1} (Yochum method) to 0.08 m^3 s^{-1} (the critical flow method) [*Moody*, 2016]. The arithmetic mean of the indirect estimates for the four methods was 0.057 ± 0.020 m^3 s^{-1} m, which is a unit area peak surface runoff of 6.8 ± 2.4 m^3 s^{-1} km^{-2} assuming an area of 8440 m^2. The indirect estimate of peak surface runoff may have been associated with the peak rainfall rate on 12 September (5 min rainfall intensity of 43.7 mm h^{-1}). The magnitude of the indirectly estimated peak surface runoff for the research area was not unprecedented; it was similar to measured peak surface runoff values at the site during the first 2 years after the wildfire for similar 5 min peak rainfall intensities. For example, a 5 min peak rainfall intensity of 79.8 mm h^{-1} on 7 July 2011 produced a peak runoff at the 3 inch, modified Parshall flume of >0.045 m^3 s^{-1} (>5.3 m^3 s^{-1} km^{-2}) [*Rengers et al.*, 2016], and a 5 min peak intensity of 53.1 mm h^{-1} on 12 July 2012 produced 0.031 m^3 s^{-1} (3.7 m^3 s^{-1} km^{-2}). Soil-water content measurements at 5 cm depth from the automated sensors that show delayed, downward propagating wetting fronts and the short rain storm durations during these 2011 and 2012 examples suggest that surface runoff generation was by the infiltration-excess mechanism during these 2011 and 2012 storms.

Our estimated unit area peak surface runoff ($\sim$6.8 m^3 s^{-1} km^{-2}) was slightly greater than unit area peak surface runoff after wildfire in the Rocky Mountains reported by *Kunze and Stednick* [2006] of 3.9 m^3 s^{-1} km^{-2} (Colorado), by *Campbell et al.* [1977] of 4.1 m^3 s^{-1} km^{-2} (Arizona), and by *Bolin and Ward* [1987] of 3.2 m^3 s^{-1} km^{-2} (New Mexico). It was, however, below the limit of maximum postwildfire unit peak surface runoff for large watersheds reported by *Moody and Martin* [2001a] and *Moody* [2012] in the Western US for watersheds $\sim$20 km^2 of 24–50 m^3 s^{-1} km^{-2}. The estimated value for our research area was relatively close to the mean unit area peak surface runoff for flash floods (5.6 m^3 s^{-1} km^{-2}) for burned watersheds using the data from *Gartner et al.* [2004].

3.5. Simulated Surface Runoff With Spatially Uniform Surface (0–3 cm) Soil K_f

There were clear differences in simulated surface runoff between the burned and unburned areas for a spatially uniform K_f between 0 and 3 cm soil depth. The simulation of the burned area with K_f equal to the geometric mean showed distinct periods of surface runoff generation associated with higher rainfall rates from 23:00 to 2:00 MDT 11–12 September and 21:00–23:30 MDT 12 September (Figures 3 and 6A–6D). The peak simulated surface runoff (0.043 m^3 s^{-1}, approximately 1:15 MDT on 12 September, Figure 6B) was larger than the later peak (0.015 m^3 s^{-1}, approximately 21:40 MDT on 12 September, Figure 6D) and was likely the approximate time of peak surface runoff for this burned catchment. The simulated peak surface runoff (0.043 m^3 s^{-1}) was within one standard deviation of the indirect peak surface runoff (0.057 m^3 s^{-1}). The most striking feature of Figures 6B and 6D was the absence of simulated surface runoff in the unburned area for the case of the spatially uniform K_f between 0 and 3 cm soil depth set to the geometric mean. Even
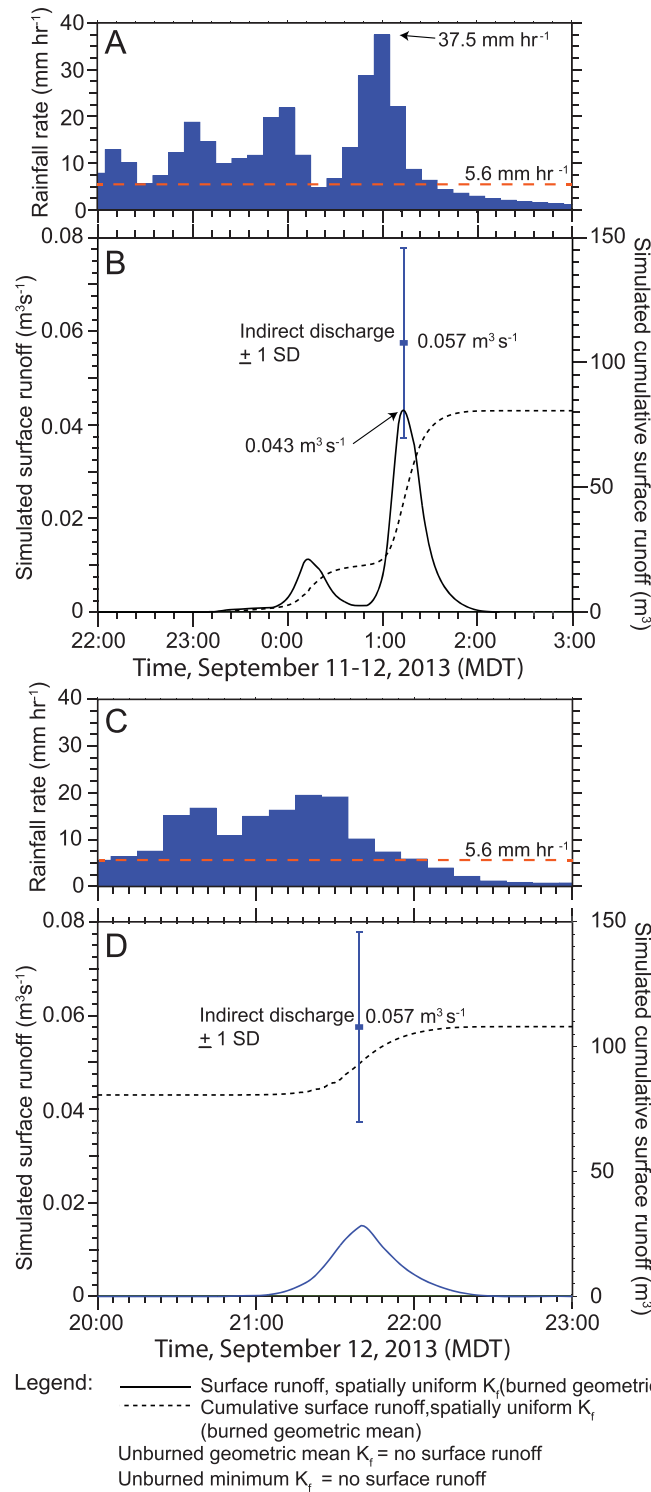
Figure 6. (A) 10 min rainfall rate, 22:00–3:00 MDT, 11–12 September. (B) Simulated surface runoff for the spatially uniform K_f simulation using the geometric mean of the burned K_f from 0 to 3 cm, 22:00–3:00 MDT, 11–12 September. (C) 10 min rainfall, 20:00–23:00 on 12 September. (D) Simulated surface runoff for the spatially uniform K_f simulation using the geometric mean of the burned K_f from 0 to 3 cm, 20:00–23:00 on 12 September. Note that 0.01 $m^3 s^{-1}$ is approximately 4.3 mm h^{-1} of surface runoff.

with the spatially uniform K_f between 0 and 3 cm soil depth set to the minimum measured unburned K_f of 81.9 mm h^{-1} (Table 2), no surface runoff was simulated during the period of the September 2013 storms. In the unburned simulations, all rainfall became subsurface flow and deep percolation into the weathered bedrock. It should be noted that the unburned simulation did not have a layer of litter/duff atop the soil, that the rainfall in the unburned case did not have any interception losses (i.e., it is the same as the burned simulation), and used the same Manning's roughness to focus on the shifts in soil-hydraulic properties resulting from fire effects. The simulated surface runoff results indicated a clear difference in simulated hydrologic response between burned and unburned areas 3 years after disturbance by wild-fire in response to an extreme rain storm as a result of soil-hydraulic property differences resulting from persistent wildfire effects (Table 2). The burned area generated infiltration-excess sur-face runoff while the unburned catchment did not generate surface runoff and all rainfall became subsurface flow (see sec-tion 3.8 below for supportive evi-dence based on soil saturation).

3.6. Simulated Runoff Sensitivity to Manning's Roughness

Surface hydraulic roughness is one of the most challenging parameters to accurately charac-terize in runoff modeling, espe-cially in wildfire-affected areas. Runoff was simulated first with a spatially uniform K_f equal to the geometric mean for the burned site. Then runoff was simulated for three values of Manning's roughness (0.21 s m$^{-1/3}$, which was the average of hillslope

measurements at the site, 0.13 s m$^{-1/3}$, the lowest measured value, and 0.29 s m$^{-1/3}$, the highest measured value; Figures 7B and 7D). Peak surface runoff differences between the Manning's roughness simulations were moderate (0.052–0.037 m^3 s^{-1} for roughness equal to 0.13 and 0.29, respectively). As expected from theory, lower roughness led to faster hydrograph rises and higher peak surface runoff (Figures 7B and 7D). Unburned Manning's roughness sensitivity is not shown in Figure 7 because no surface runoff was simulated. Hydraulic roughness parameterization differences slightly changed surface runoff timing and moderately change peak surface runoff.

The Manning's roughness values used here were generally consistent with those estimated by model calibration or measurement for forested, burned watersheds. *Canfield et al.* [2005] calibrated a hydrologic response model in a burned forested watershed using observed hydrographs to estimate Manning's roughness and found values ranging from 0.011 about 1 month after the fire to 1.05 more than 3 years after the fire. *Rulli and Rosso* [2007] used 0.05 s m$^{-1/3}$ for Manning's roughness on chaparral hillslopes in their post-wildfire hydrologic simulations, although it was not clear how this value was estimated. *Stoof et al.* [2015] noted that fire significantly reduced Manning's roughness on a shrubland hillslope from 0.64 ± 0.18 prefire to 0.28 ± 0.11 postfire, based on field measurements. Manning's roughness values used in this work were similar to the values measured by *Stoof et al.* [2015], greater than the value used by *Rulli and Rosso* [2007], but much less than the 3 year postfire values from *Canfield et al.* [2005]. Clearly, Manning's roughness depends on surface conditions, including vegetation recovery, and may also vary spatially after wildfire [e.g., *Lavee et al.*, 1995; *Kutiel et al.*, 1995] depending on the flow depth.
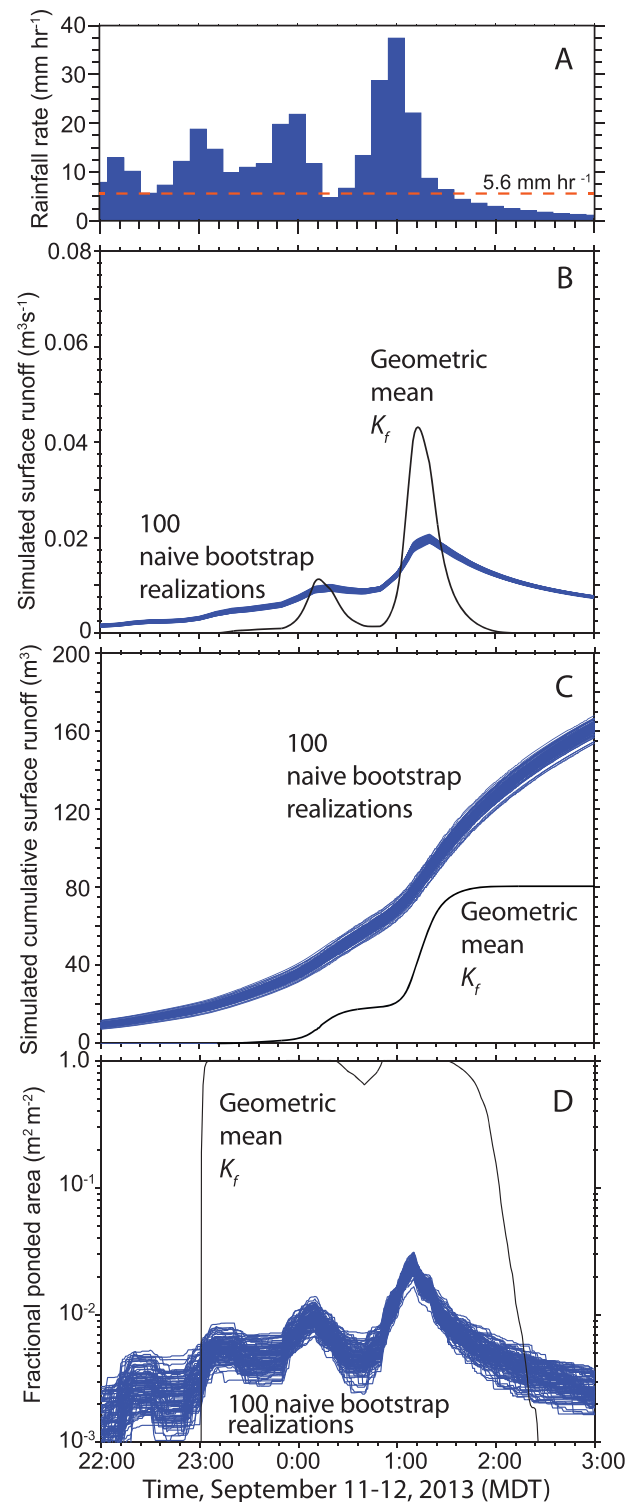
3.7. Simulated Surface Runoff With Spatially Variable Surface (0–3 cm) K_f

All 100 of the simulated runoff hydrographs for the burned area with spatially variable K_f had lower magnitudes but were more temporally pervasive than the surface runoff for spatially uniform K_f (geometric mean). The spread of simulated peak surface runoff values for the spatially variable K_f case was relatively small (Figure 8B), with a mean of 0.020 m^3 s^{-1} and a range (i.e., least to greatest) of 0.019–0.021 m^3 s^{-1} suggesting that the variability within the 100 realizations was not a strong control on variability in simulated surface runoff generation. Peak simulated runoff values from the spatially variable K_f realizations were all less than the spatially uniform K_f simulation, indicating strong "run-on" controls on runoff generation in the spatially variable K_f realizations. The opposite trend was observed in cumulative surface runoff, where the spatially uniform K_f simulation produced a total surface runoff of 80 m^3 and the spatially variable K_f simulations produced total surface runoff of 155–165 m^3, approximately twice as large (Figure 8C). The greater total surface runoff for the spatially variable K_f simulations, despite lower peak simulated surface runoff, resulted from a much longer period of substantial runoff generation (Figure 8B). The fractional ponded area, ranging from 0 to 1 with 1 being the total area, was an indication of the contributing area and showed a clear threshold surface saturation response for the spatially uniform K_f simulation when rainfall rate exceeds infiltration rate, while the 100 spatially variable simulations had less than 5% surface saturation, indicating much smaller but more persistent contributing areas associated with connected, near-channel low K_f areas. Further confirmation of the role of different contributing areas was provided by maps of surface water depth and surface saturation at the time of simulated peak surface runoff for both uniform and spatially variable K_f simulations (Figure 9). The spatially variable K_f case was for realization 48, which had the greatest peak simulated surface runoff of the spatially variable simulations in Figure 8. The spatially uniform K_f simulation had surface water depths strongly controlled by topography, with sheet flow over the hillslope and concentrated flow in the hollow, and nearly the entire catchment area was contributing at the time of peak surface runoff. In contrast, the spatially variable K_f simulation had patchy areas of substantial surface water depth that did not concentrate into larger depths until nearly at the catchment outlet where the depth is about 0.063 m and similar to the reach average hydraulic radius (0.074 m [*Moody*, 2016]) for the indirect discharge measurement. Surface saturations were low except in isolated K_f low areas that connect further downslope near the catchment outlet (Figure 9).
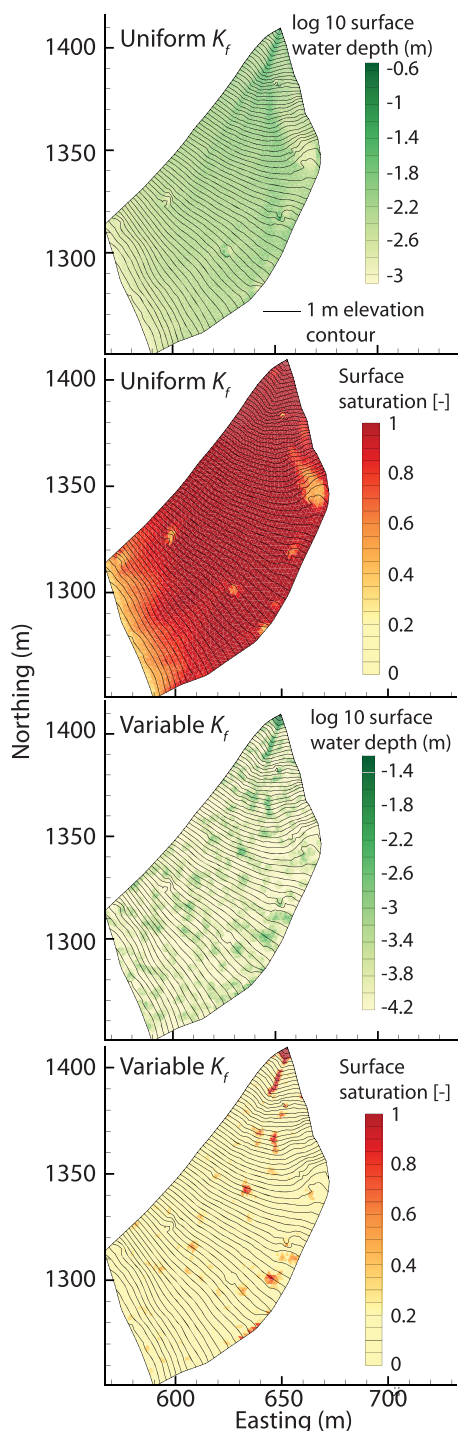
Overall, the differences suggest, for the spatially uniform K_f simulation, an "all or nothing" threshold response driven by rainfall rate exceeding infiltration capacity; the contributing area was nearly the entire simulated catchment at the time of peak surface runoff. In contrast, for the spatially varying K_f, there were more gradual transitions in runoff generation driven by spatial connectivity in saturated areas where rainfall rate exceeded infiltration rate including the need to overcome "run-on" losses as surface water was lost to the subsurface. Contributing areas were patchy in the spatially varying K_f simulations with high K_f areas
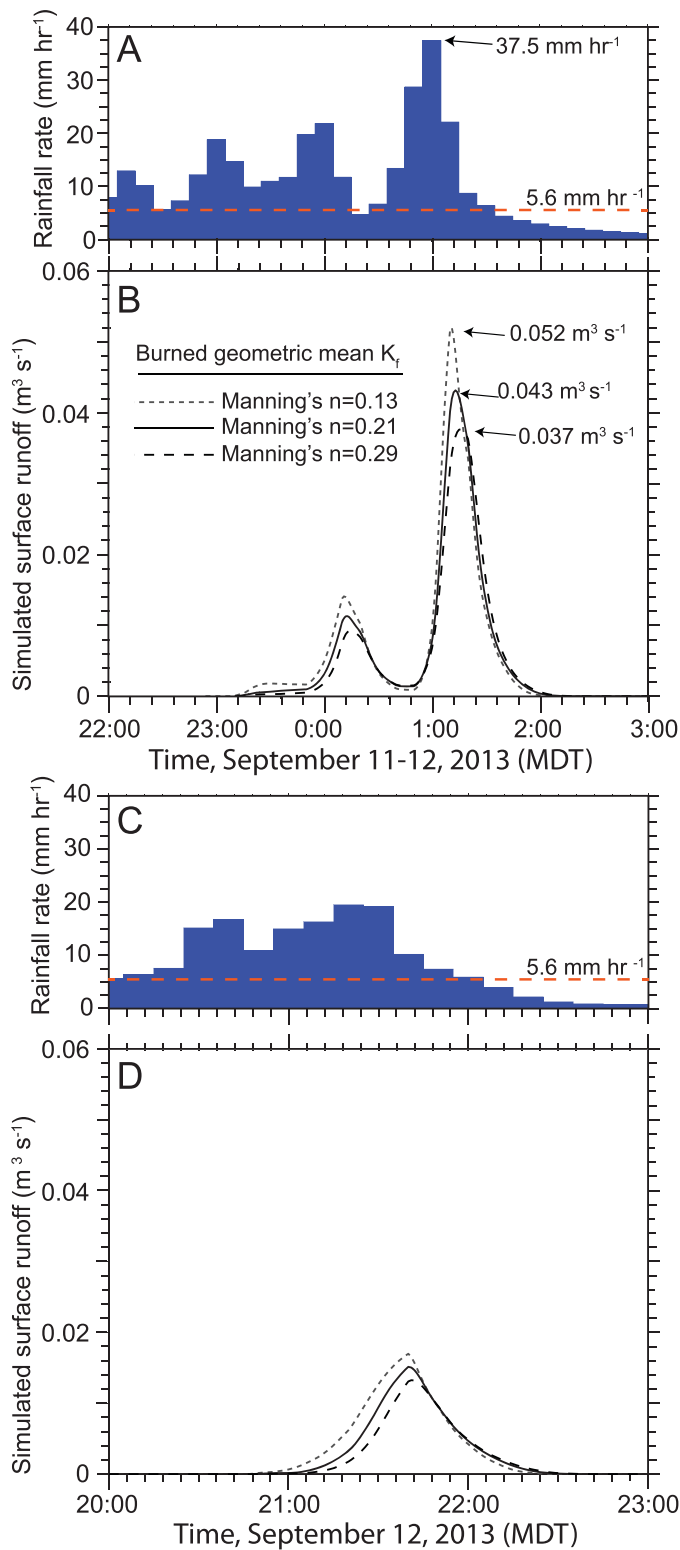
Figure 7. (A) 10 min rainfall, 22:00–3:00 MDT, 11–12 September. (B) Simulated surface runoff for the spatially uniform K_f simulation using the geometric mean of the burned K_f (Table 2) with different values of Manning's roughness, 22:00–3:00 MDT, 11–12 September. (C) 10 min rainfall, 20:00–23:00 on 12 September. (D) Simulated surface runoff for the spatially uniform K_f simulation using the geometric mean of the burned K_f with different values of Manning's roughness, 20:00–23:00 on 12 September. Note that 0.01 m^3 s^{-1} is approximately 4.3 mm h^{-1} of surface runoff.

Figure 8. (A) 10 min rainfall rate. (B) Simulated surface runoff for the spatially uniform K_f simulation using the geometric mean (Table 2) of the burned K_f and 100 spatially variable K_f realizations. Note that 0.01 m^3 s^{-1} is approximately 4.3 mm h^{-1} of surface runoff. (C) Simulated cumulative surface runoff for the spatially uniform K_f simulation using the geometric mean of the burned K_f and 100 spatially variable K_f simulations. (D) The fractional ponded area for the spatially uniform K_f simulation using the geometric mean of the burned K_f and 100 spatially variable K_f simulations. The simulated fractional ponded area requires a surface water depth exceeding the depression storage, mobile water depth, and the height of microtopography.
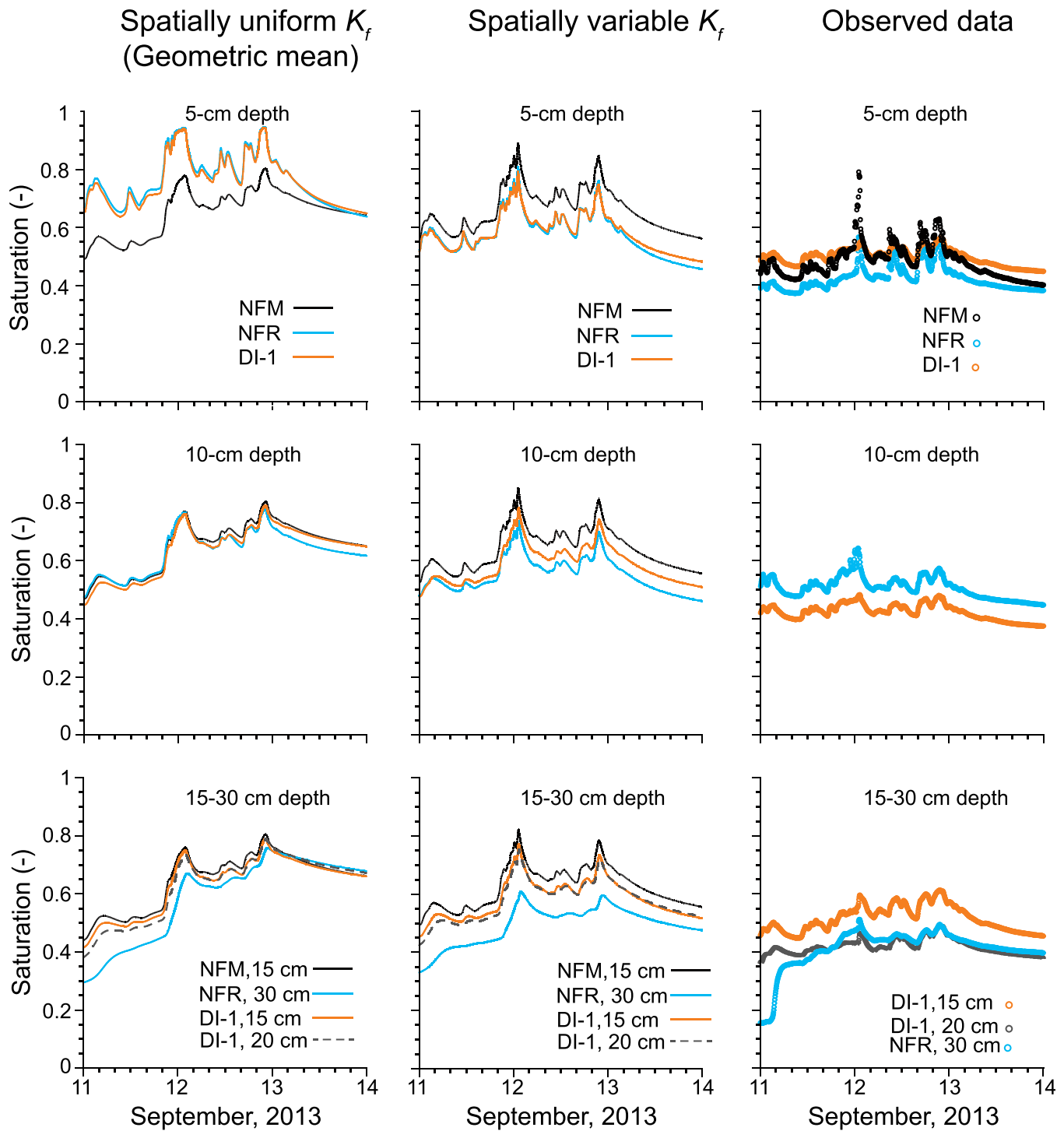
Figure 9. Simulated surface water depths and fractional saturations for the spatially uniform K_f simulation using the geometric mean of the burned K_f and a spatially variable K_f simulation (realization 48, which had the greatest peak surface runoff).

acting as "sinks" for infiltration-excess runoff generation, which then became subsurface flow. It should be noted that because the spatially uniform minimum K_f simulation for the unburned area did not generate surface runoff, spatially variable K_f for the unburned area was not considered.

3.8. Simulated Soil Saturation

Simulated and observed subsurface saturation supported infiltration-excess as the dominant surface runoff generation mechanism in this burned headwater catchment during the September 2013 storms. Because neither the unburned simulations nor the unburned saturation data [*Ebel et al.*, 2015] suggested infiltration-excess overland flow, those results were not analyzed here and the focus was on the burned simulations. Neither the simulations nor the observations reached saturated conditions (i.e., 1) at 5 cm depth or deeper during the September 2013 storms (9–17 September) (Figure 10 and Table 3). The observed fractional (i.e., 0–1) peak saturations in the soil were all below 0.65, with the exception of the 5 cm deep sensor at the NFM location, which was 0.79 (Figure 10 and Table 3). The simulated maximum fractional saturations were closer to 1, but only at the 5 cm depth (Table 3). The lack of saturated soil at depth, and the decreasing saturation with increasing depth (Figure 10 and Table 3), pointed strongly to downward propagating saturation profiles associated with infiltration-excess runoff. It should be noted that the simulated points were nominally at the listed depths (i.e., the closest finite-element node), which affected some of the trends shown in Figure 10. For example, the delayed response of the NFM 5 cm simulated point in the geometric mean K_f simulation was the result of that node being 6.5 cm below the surface while the nodes representing the NFR and DI-1 simulations were closer to 3 cm below the surface and just below the lower K_f soil layer between 0 and 3 cm depth. This explained the higher saturations for NFR and DI-1 in that simulation. Also, the spatially variable K_f simulation shown in Figure 10 tended to have a "spikier," more dynamic saturation time series compared to the spatially uniform K_f simulation, and tended to better mimic the observed time series behavior. This may be the result of that particular K_f realization having relatively high K_f values

at the surface at the NFM (126 mm h^{-1}), NFR (90 mm h^{-1}), and DI-1 (282 mm h^{-1}) locations. The higher K_f values allowed the rainfall temporal variability to affect the subsurface more than the spatially uniform K_f simulation, with the lower K_f acting like a low-pass filter and eliminating rainfall temporal variability when the rainfall rate exceeds infiltration capacity. In burned areas with spatially variable K_f, high-frequency temporal variability

Figure 10. Simulated and observed saturations at the NFM, NFR, and DI-1 locations (see Figure 2). Simulated fractional saturations are from the spatially uniform K_f simulation using the geometric mean of the burned K_f and the spatially variable K_f simulation is for realization 48, which had the greatest peak surface runoff (same as shown in Figure 9).

in subsurface saturation observed by in situ sensors may indicate areas of relatively high K_f while a temporally "damped" response would indicate that an overlying low K_f near-surface region was present.

3.9. Discussion of Simulated Surface Runoff With Spatially Variable K_f

Numerous computational modeling investigations have examined infiltration-excess runoff generation with spatially variable K_f in nonwildfire affected areas [e.g., *Freeze*, 1980; *Luce and Cundy*, 1994; *Saghafian et al.*,

Table 3. Maximum Saturations Reached During Uniform K_f Simulation Using the Geometric Mean of the Burned K_f, the Spatially Variable K_f Simulation With the Maximum Peak Surface Runoff (Realization 48), and Observations From In Situ Soil-Water Content Sensors

Observation Location	Depth (cm)	Geometric Mean K_f, Burned Maximum Saturation	Spatially Variable K_f, Burned Maximum Saturation	Observed Maximum Saturation
NFM	5	0.80	0.89	0.79
	10	0.80	0.85	Malfunctioned
	15	0.81	0.82	Malfunctioned
NFR	5	0.94	0.81	0.57
	10	0.78	0.74	0.64
	30	0.76	0.61	0.51
DI-1	5	0.94	0.79	0.56
	10	0.79	0.78	0.48
	15	0.79	0.77	0.61
	20	0.79	0.75	0.49

1995; *Smith and Goodrich*, 2000; *Herbst et al.*, 2006; *Nahar et al.*, 2004; *Maxwell and Kollet*, 2008]. Conclusions from these investigations indicated that spatially uniform K_f simulations overestimated runoff for high rainfall rates and underestimated runoff for low rainfall rates [e.g., *Goodrich et al.*, 1994; *Smith et al.*, 1995]. Models based on spatially variable K_f also showed that runoff took place earlier and increased more gradually than would be the case with spatially uniform K_f as higher infiltration capacity areas contributed surface runoff later [*Smith and Hebbert*, 1979; *Luce and Cundy*, 1994]. Finally, we know that spatial variability in K_f had a larger effect for smaller rainfall rates (those just above the threshold for infiltration-excess runoff generation), while at higher rainfall rates, runoff generation was less sensitive to spatial variation in K_f [e.g., *Smith and Goodrich*, 2000; *Ogden et al.*, 2000]. A few studies have considered fully three-dimensional variability in K_f [*Maxwell and Kollett*, 2008; *Meyerhoff and Maxwell*, 2011] and showed that the fraction of the saturated surface area depended on the variance of K_f and the rainfall rate and that greater variance in K_f promoted more overland flow runoff generation. *Maxwell and Kollett* [2008] showed the effect of the development of very shallow perched water lenses because of shallow low K_f zones. Because we have no field evidence to support three-dimensional K_f variability beyond the 3 cm depth of the tension infiltrometer measurements, only two-dimensional K_f variability was simulated in this work. While speculative, it seems possible, based on the work by *Maxwell and Kollett* [2008] that incorporating three-dimensional subsurface variability in K_f may increase surface runoff generation by reducing the effectiveness of "run on" areas on the hillslope. The studies listed above representing unburned areas were consistent with the findings reported here for runoff simulation in a burned area, with earlier and more prolonged runoff generation and much smaller contributing areas in spatially variable K_f simulations relative to spatially uniform K_f.

One important consideration was whether 100 realizations of K_f were sufficient to capture the K_f variability. The naïve bootstrap method of generating K_f had advantages in that it used actual measured data at the site and did not make any assumptions of a statistical distribution. The method also had the disadvantage that the number of measurements may not accurately capture the full range of variability. The variance in simulated peak surface runoff leveled off after about 20 realizations and stayed relatively consistent from 20 through 100 realizations (Figure 11), suggesting that 100 realizations was sufficient for an analysis focused on surface runoff generation mechanisms in a burned catchment.

3.10. Evolution of Surface Runoff Generation With Time Since Wildfire

Substantial increases in runoff and sediment export in the first year after wildfire are common [e.g., *Lane et al.*, 2006; *Sheridan et al.*, 2007; *Ferreira et al.*, 2008] with exponential declines in runoff and sediment yields to background levels within 2 years after the fire in some areas [*Sheridan et al.*, 2007]. The declines with time hinge, in part, on the recovery of infiltration capacity and the loss of connectivity between low infiltration capacity areas at hillslope and catchment scales [*Ferreira et al.*, 2005, 2008]. The simulated runoff generation here, primarily from near-channel low K_f areas, was strikingly similar to the runoff generation mechanism described by *Sheridan et al.* [2007] in Australian wet Eucalyptus forest. The research area focused upon here represents a transition from a highly connected low infiltration capacity system immediately after the wildfire [*Ebel et al.*, 2012] to the disconnected system 3 years after the fire that produces limited runoff primarily from near channel areas. As noted by *Robichaud* [2000], single values of K_f may not be appropriate for burned forested sites and that probability distributions better characterize variability,
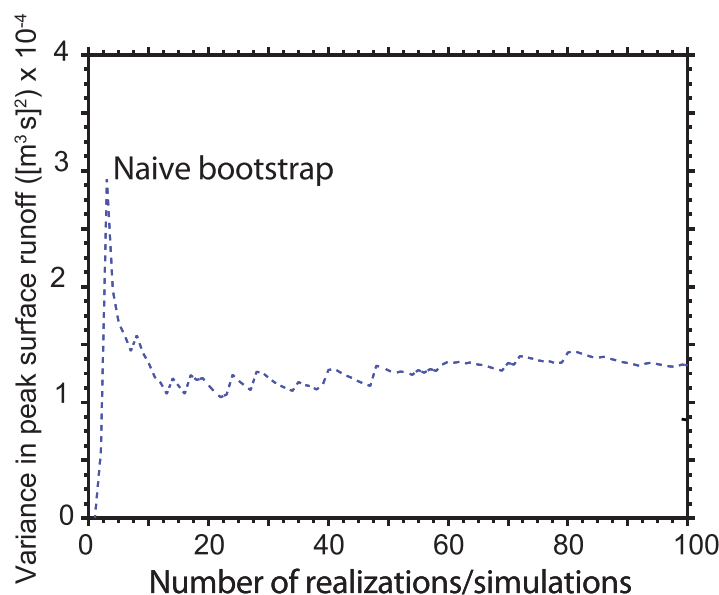
Figure 11. Variance in simulated peak surface runoff as a function of the number of realizations in the spatially variable K_f simulations.

hence the stochastic modeling approach used here. Despite the importance of the connectivity of low-infiltration areas for runoff generation and erosion [e.g., *Imeson et al.*, 1992; *Cerdà et al.*, 1998; *Prosser and Williams*, 1998; *Shakesby et al.*, 2000; *Ferreira et al.*, 2005, 2008] including soil-water repellency effects [*Coelho et al.*, 2004; *Keizer et al.*, 2005], few efforts have comprehensively characterized spatial variability at the hillslope scale. The *Woods et al.* [2007] characterization of the spatial variability of water repellency was one of the few and highlights the importance of spatial variations in infiltration determining runoff. These spatial variations in infiltration capacity are not only important the first 2 years after wildfire, they remain an important control of runoff generation processes longer after wildfire during extreme rainfall, as shown in this work.

3.11. Geomorphic Implications

One of the most striking aspects of the simulation results was the longer duration of runoff generation in the spatially variable K_f simulations. Simulated total runoff in the spatially variable K_f simulations was twice as large as the spatially uniform K_f simulation. While maximum overland flow depths and velocities may be smaller, the total duration of surface runoff may have important geomorphic implications relative to spatially uniform K_f representation. In wildfire-affected areas, sustained flow in channels has been shown to enhance mobility of coarse-grained sediment moved from hillslopes into channels by shorter duration rain storms [*Reneau et al.*, 2007; *Rengers et al.*, 2016]. It is possible that the longer duration concentrated flows in the catchment hollow, suggested by the spatially variable K_f simulations, exported coarse-grained sediment more effectively than shorter duration storms. Long duration rainfall, such as the type examined here for the 2013 September storms, sufficient to cause infiltration-excess runoff generation on spatially variable K_f areas, may entrain and export coarse-grained sediments from headwater catchments that shorter duration storms cannot accomplish. Figure 12 shows a time sequence of photographs taken at the catchment outlet (i.e., where the flume was located prior to removal). The 12 October 2010 photo (29 days postwildfire) shows the incipient channel formation in the hollow (Figure 12). The 20 June 2011 and 14 July 2011 photographs show the removal of fine sediment by runoff from convective thunderstorms and emergence of coarse sediment in the topographic hollow (see ground-based LiDAR results from *Rengers et al.* [2016]). The transition to a large cobble and boulder channel is visible in the 22 September 2013 photograph following the 2013 floods. The longer duration surface runoff during the 2013 September storms may explain the differences of geomorphic response between shorter convective storms in the year following the 2010 Fourmile Canyon wildfire and the long duration 2013 storm. If longer duration rain storms on spatially variable K_f areas produce longer duration overland flow that is more geomorphically effective than a uniform K_f surface, major implications are indicated for simulating sediment transport after wildfire with spatially uniform K_f models.

3.12. Discussion of Study Limitations

There were several important assumptions and associated limitations of this work. One limitation was that S was affected by soil moisture [e.g., *Philip*, 1957; *Stewart et al.*, 2013] and prestorm soil-moisture conditions were not identical to the soil-moisture conditions at the time of sampling 2 months following the storm. The mean soil-water content (0–3 cm depth) when soil-hydraulic properties were measured was 0.084

Figure 12. Time series of photographs near the headwater catchment outlet where the surface runoff flume was located prior to removal. The pink shaded rocks mark common points between the photographs for comparison of changes in channel morphology and the emergence of cobbles and boulders. The 2013 photograph was taken by J. Moody.

(burned) and 0.183 (unburned). Soil-water content data from the automated sensors at 5 cm depth before the extreme rainfall event on 1 September 2013 was 0.082 (average of three sensors) in the burned area and 0.071 in the unburned area, suggesting that S was underestimated in the unburned area relative to conditions prior to the 2013 storm. An additional assumption was the use of tension infiltrometer measurements (-1 cm applied pressure head) to represent K_f. The -1 cm pressure head will exclude flow through the largest pores, such as macropores, and therefore potentially underestimate K_f. The tension infiltrometer measurements were used to represent K_f because these measurements include the effect of soil-water repellency, which would be overwhelmed by ponded head infiltration measurements [see *Nyman et al.*, 2010; *Ebel et al.*, 2012]. If the tension infiltrometer measurements underestimate K_f then the simulated surface runoff would be overestimated, which does not appear to be the case based on Figure 6. The assumption was also made that the extreme rainfall itself did not affect the soil surface soil-hydraulic properties differently for the burned versus unburned areas. Soil sealing is a postwildfire process that could cause within-storm reductions in soil-hydraulic properties that affect infiltration [*Campbell et al.*, 1977; *Neary et al.*, 1999; *Larsen et al.*, 2009]. Without immediate prestorm infiltration measurements, it is not possible to rule this out and thus the infiltration measurements in the burned area taken after the extreme rainfall may represent values more representative of the peak of the extreme rainfall rather than at the initiation of the storm.

4. Conclusions

Hydrologic legacies of landscape disturbances such as wildfire impact hydrologic response during extreme rainfall events in headwater catchments. Field measurements of soil-hydraulic properties and soil-water water repellency showed substantial differences between burned and unburned soils despite 3 years of recovery after wildfire. These differences in soil-hydraulic properties impacted the hydrologic response and runoff generation during the extreme rainfall in September 2013 in the Colorado Front Range, causing simulated surface runoff by the infiltration-excess mechanism in the burned area while no simulated surface runoff was generated in the unburned area. Indirect field estimates of peak discharge confirmed the magnitude of the simulated peak surface runoff within the sensitivity of Manning's roughness estimates. Spatially variable K_f hydrologic response simulations produced longer duration but lower peak-flow infiltration-excess runoff compared to uniform K_f simulations. Contributing areas and thresholds of runoff generation were quite different between the spatially uniform and spatially variable simulations. Spatially variable K_f simulations produced twice as much total surface runoff over the same time period as the spatially uniform K_f simulation. Surface runoff differences between spatially uniform and spatially variable K_f simulations may have major hillslope sediment export implications during long duration, extreme rainfall events such as the 2013 September storms in the Colorado Front Range. These results suggest that long duration storms on

landscapes recovering from disturbance that possess spatial variability in soil-hydraulic parameters may produce major geomorphic changes resulting from sustained sediment export.

References

Balfour, V. N., and S. W. Woods (2013), The hydrological properties and the effects of hydration on vegetative ash from the Northern Rockies, USA, *Catena*, *111*, 9–24.

Balfour, V. N., S. H. Doerr, and P. R. Robichaud (2014), The temporal evolution of wildfire ash and implications for post-fire infiltration, *Int. J. Wildland Fire*, *23*(5), 733–745.

Benavides-Solorio, J., and L. H. MacDonald (2001), Post-fire runoff and erosion from simulated rainfall on small plots, Colorado Front Range, *Hydrol. Processes*, *15*, 2931–2952.

BeVille, S. H., B. B. Mirus, B. A. Ebel, G. G. Mader, and K. Loague (2010), Using simulated hydrologic response to revisit the 1973 Lerida Court landslide, *Environ. Earth Sci.*, *61*(6), 1249–1257.

Birkeland, P. W., R. R. Shroba, S. F. Burns, A. B. Price, and P. J. Tonkin (2003), Integrating soils and geomorphology in mountains—An example from the Front Range of Colorado, *Geomorphology*, *55*, 329–344.

Bodí, M. B., J. Mataix-Solera, S. H. Doerr, and A. Cerdà (2011), The wettability of ash from burned vegetation and its relationship to Mediterranean plant species type, burn severity and total organic carbon content, *Geoderma*, *160*(3), 599–607.

Bodí, M. B., S. H. Doerr, A. Cerdà, and J. Mataix-Solera (2012), Hydrological effects of a layer of vegetation ash on underlying wettable and water repellent soil, *Geoderma*, *191*, 14–23.

Bolin, S. B., and T. J. Ward (1987), Recovery of a New Mexico drainage basin from a forest fire, *IAHS AISH Publ. 167*, 191–198.

Borga, M., M. Stoffel, L. Marchi, F. Marra, and M. Jakob (2014), Hydrogeomorphic response to extreme rainfall in headwater systems: Flash floods and debris flows, *J. Hydrol.*, *518*, 194–205.

Brown, J. A. H. (1972), Hydrologic effects of a brushfire in a catchment in south-eastern New South Wales, *J. Hydrol.*, *15*, 77–96.

Campbell, R. E., P. F. Baker, P. F. Folliot, F. R. Larson, and C. C. Avery (1977), Wildfire effects on a ponderosa pine ecosystem: An Arizona case study, USDA For. Serv. Res. Pap. RM-191, U.S. Dep. of Agric., U.S. For. Serv., Fort Collins, Colo.

Canfield, H. E., D. C. Goodrich, and I. S. Burns (2005), Selection of parameter values to model post-fire runoff and sediment transport at the watershed scale in southwestern forests, in *Proceedings of ASCE Watershed Management Conference*, pp. 19–22, Am. Soc. of Civ. Eng., Reston, Va.

Carr, A. E., K. Loague, and J. E. VanderKwaak (2014), Hydrologic-response simulations for the North Fork of Caspar Creek: Second-growth, clear-cut, new-growth, and cumulative watershed effect scenarios, *Hydrol. Processes*, *28*(3), 1476–1494.

Cerdà, A. (1998), Changes in overland flow and infiltration after a rangeland fire in a Mediterranean scrubland, *Hydrol. Processes*, *12*, 1031–1042.

Cerdà, A., and S. H. Doerr (2005), Influence of vegetation recovery on soil hydrology and erodibility following fire: An 11-year investigation, *Int. J. Wildland Fire*, *14*(4), 423–437.

Cerdà, A., and S. H. Doerr (2008), The effect of ash and needle cover on surface runoff and erosion in the immediate post-fire period, *Catena*, *74*, 256–263, doi:10.1016/j.catena.2008.03.010.

Cerdà, A., and P. Robichaud (2009), Fire effects on soil infiltration, in *Fire Effects on Soils and Restoration Strategies*, edited by A. Cerdà and P. Robichaud, chap. 3, pp. 81–103, Sci. Publ., Enfield, N. H.

Cerdà, A., S. Schnabel, A. Ceballos, and D. Gomez-Amelia (1998), Soil hydrological response under simulated rainfall in the Dehesa land system (Extremadura, SW Spain) under drought conditions, *Earth Surf. Processes Landforms*, *23*, 195–209.

Chow, V. T. (1959), *Open-Channel Hydraulics*, 680 pp., McGraw-Hill, New York.

Cobos, D. R., and C. Campbell (2007), Correcting temperature sensitivity of ECH2O soil moisture sensors, *Appl. Note Rep. 13394-02 AN*, Decagon Devices, Pullman, Wash.

Cobos, D. R., and C. Chambers (2010), *Calibrating ECH2O Soil Moisture Sensors*, 7 pp., Decagon Devices, Pullman, Wash.

Coe, J. A., J. W. Kean, J. W. Godt, R. L. Baum, E. S. Jones, D. J. Gochis, and G. S. Anderson (2014), New insights into debris-flow hazards from an extraordinary event in the Colorado Front Range, *GSA Today*, *24*, 4–10, doi:10.1130/GSATG214A.1.

Coelho, C. D. O. A., A. J. D. Ferreira, A. K. Boulet, and J. J. Keizer (2004), Overland flow generation processes, erosion yields and solute loss following different intensity fires, *Q. J. Eng. Geol. Hydrogeol.*, *37*, 233–240.

Comiti, F., L. Mao, A. Wilcox, E. E. Wohl, and M. A. Lenzi (2007), Field-derived relationships for flow velocity and resistance in high-gradient streams, *J. Hydrol.*, *340*, 48–62.

Curriero, F. C., J. A. Patz, J. B. Rose, and S. Lele (2001), The association between extreme precipitation and waterborne disease outbreaks in the United States, 1948-1994, *Am. J. Public Health*, *91*(8), 1194–1199.

Decagon Devices (2006), *Mini Disk Infiltrometer User's Manual*, Pullman, Wash.

Dekker, L. W., C. J. Ritsema, K. Oostindie, D. Moore, and J. G. Wesseling (2009), Methods for determining soil water repellency on field-moist samples, *Water Resour. Res.*, *45*, W00D33, doi:10.1029/2008WR007070.

Doerr, S. H., and A. D. Thomas (2000), The role of soil moisture in controlling water repellency: New evidence from forest soils in Portugal, *J. Hydrol.*, *231*, 134–147.

Doerr, S. H., R. A. Shakesby, and R. P. D. Walsh (2000), Soil water repellency: Its causes, characteristics and hydro-geomorphological significance, *Earth Sci. Rev.*, *51*, 33–65, doi:10.1016/S0012-8252(00)00011-8.

Easterling, D. R., G. A. Meehl, C. Parmesan, S. A. Changnon, T. R. Karl, and L. O. Mearns (2000), Climate extremes: Observations, modeling, and impacts, *Science*, *289*, 2068–2074.

Ebel, B. A. (2012), Wildfire impacts on soil-water retention in the Colorado Front Range, United States, *Water Resour. Res.*, *48*, W12515, doi:10.1029/2012WR012362.

Ebel, B. A. (2013a), Wildfire and aspect effects on hydrologic states after the 2010 Fourmile Canyon Fire, *Vadose Zone J.*, *12*, 1–19, doi:10.2136/vzj2012.0089.

Ebel, B. A. (2013b), Simulated unsaturated flow processes after wildfire and interactions with slope aspect, *Water Resour. Res.*, *49*, 8090–8107, doi:10.1002/2013WR014129.

Ebel, B. A., and B. B. Mirus (2014), Disturbance hydrology: Challenges and opportunities, *Hydrol. Processes*, *28*, 5140–5148.

Ebel, B. A., B. B. Mirus, C. S. Heppner, J. E. VanderKwaak, and K. Loague (2009), First-order exchange coefficient coupling for simulating surface water–groundwater interactions: Parameter sensitivity and consistency with a physics-based approach, *Hydrol. Processes*, *23*, 1949–1959.

Ebel, B. A., J. A. Moody, and D. A. Martin (2012), Hydrologic conditions controlling runoff generation immediately after wildfire, *Water Resour. Res.*, *48*, W03529, doi:10.1029/2011WR011470.

Ebel, B. A, F. K. Rengers, and G. E. Tucker (2015), Aspect-dependent soil saturation and insight into debris-flow initiation during extreme rainfall in the Colorado Front Range, *Geology*, *43*, 659–662, doi:10.1130/G36741.1.

Efron, B. (1979), Bootstrap methods: Another look at the jackknife, *Ann. Stat.*, *7*, 1–26, doi:10.1214/aos/1176344552.

Ferreira, A. J. D., C. D. O. Coelho, A. K. Boulet, G. Leighton-Boyce, J. J. Keizer, and C. J. Ritsema (2005), Influence of burning intensity on water repellency and hydrological processes at forest and shrub sites in Portugal, *Soil Res.*, *43*, 327–336.

Ferreira, A. J. D., C. D. O. Coelho, C. J. Ritsema, A. K. Boulet, and J. J. Keizer (2008), Soil and water degradation processes in burned areas: Lessons learned from a nested approach, *Catena*, *74*, 273–285.

Freeze, R. A. (1980), A stochastic-conceptual analysis of rainfall-runoff processes on a hillslope, *Water Resour. Res.*, *16*, 391–408.

Freeze, R. A., and J. A. Cherry (1979), *Groundwater*, Prentice-Hall, Englewood Cliffs, N. J.

Gable, D. J. (1980), Geologic map of the Gold Hill quadrangle, Boulder County, Colorado, *Geol. Quadrangle Map GQ-1525*, scale 1:24,000. U.S. Geol. Surv., Reston, Va.

Gartner, J. E., E. R. Bigio, and S. H. Cannon (2004), Compilation of post wildfire runoff-event data from the Western United States, *U.S. Geol. Surv. Open File Rep.*, *04-1085*, 22 pp.

Gochis, D., et al. (2015), The Great Colorado flood of September 2013, *Bull. Am. Meteorol. Soc.*, *96*, 1461–1487, doi:10.1175/BAMS-D13-00241.1.

Goodrich, D. C., T. J. Schmugge, T. J. Jackson, C. L. Unkrich, T. O. Keefer, R. Parry, L. B. Bach, and S. A. Amer (1994), Runoff simulation sensitivity to remotely sensed initial soil water content, *Water Resour. Res.*, *30*, 1393–1405.

HDSC (2013), *Exceedance Probability Analysis for the Colorado Flood Event, 9–16 September 2013*, 5 pp., Hydrometeorol. Des. Stud. Cent., Natl. Weather Serv., Silver Spring, Md.

Heppner, C. S., and K. Loague (2008), A dam problem: Simulated upstream impacts for a Searsville-like watershed, *Ecohydrology*, *1*(4), 408–424.

Herbst, M., B. Diekkruger, and J. Vanderborght (2006), Numerical experiments on the sensitivity of runoff generation to the spatial variation of soil hydraulic properties, *J. Hydrol.*, *326*, 43–58.

Holmgren, M., et al. (2006), Extreme climatic events shape arid and semiarid ecosystems, *Front. Ecol. Environ.*, *4*(2), 87–95.

Huffman, E. L., L. H. MacDonald, and J. D. Stednick (2001), Strength and persistence of fire-induced soil hydrophobicity under ponderosa and lodgepole pine, Colorado Front Range, *Hydrol. Processes*, *15*, 2877–2892.

Imeson, A. C., J. M. Verstraten, E. J. Van Mulligen, and J. Sevink (1992), The effects of fire and water repellency on infiltration and runoff under Mediterranean type forest, *Catena*, *19*, 345–361.

Inbar, M., M. Tamir, and L. Wittenberg (1998), Runoff and erosion processes after a forest fire in Mount Carmel, a Mediterranean area, *Geomorphology*, *24*(1), 17–33.

Jones, J. P., E. A. Sudicky, and R. G. McLaren (2008), Application of a fully-integrated surface-subsurface flow model at the watershed-scale: A case study, *Water Resour. Res.*, *44*, W03407, doi:10.1029/2006WR005603.

Jordán, A., L. M. Zavala, J. Mataix-Solera, A. L. Nava, and N. Alanís (2011), Effect of fire severity on water repellency and aggregate stability on Mexican volcanic soils, *Catena*, *84*(3), 136–147.

Kean, J. W., D. M. Staley, and S. H. Cannon (2011), In situ measurements of post-fire debris flows in southern California: Comparisons of the timing and magnitude of 24 debris-flow events with rainfall and soil moisture conditions, *J. Geophys. Res.*, *116*, F04019, doi:10.1029/2011JF002005.

Keizer, J. J., C. O. A. Coelho, R. A. Shakesby, C. S. P. Domingues, M. C. Malvar, I. M. B. Perez, M. J. S. Matias, and A. J. D. Ferreira (2005), The role of soil water repellency in overland flow generation in pine and eucalypt forest stands in coastal Portugal, *Soil Res.*, *43*, 337–349.

Kharin, V. V., F. W. Zwiers, X. Zhang, and G. Hegerl (2007), Changes in temperature and precipitation extremes in the IPCC ensemble of global coupled model simulations, *J. Clim.*, *20*, 1419–1444, doi:10.1175/JCLI4066.1.

Kinner, D. A., and J. A. Moody (2008), Infiltration and runoff measurements on steep burned hillslopes using a rainfall simulator with variable rain intensities, *U.S. Geol. Surv. Sci. Invest. Rep.*, *2007-5211*, 64 p.

Kinner, D. A., and J. A. Moody (2010), Spatial variability of steady-state infiltration into a two-layer soil system on burned hillslopes, *J. Hydrol.*, *381*, 322–332.

Korup, O., and J. J. Clague (2009), Natural hazards, extreme events, and mountain topography, *Quat. Sci. Rev.*, *28*(11), 977–990.

Kunze, M. D., and J. D. Stednick (2006), Streamflow and suspended sediment yield following the 2000 Bobcat fire, Colorado, *Hydrol. Processes*, *20*, 1661–1681.

Kutiel, P., H. Lavee, M. Segev, and Y. Benyamini (1995), The effect of fire-induced surface heterogeneity on rainfall-runoff-erosion relationships in an eastern Mediterranean ecosystem, Israel, *Catena*, *25*, 77–87.

Lane, P. N. J., G. J. Sheridan, and P. J. Noske (2006), Changes in sediment loads and discharge from small mountain catchments following wildfire in south eastern Australia, *J. Hydrol.*, *331*, 495–510.

Larsen, I. J., L. H. MacDonald, E. Brown, D. Rough, M. J. Welsh, J. H. Pietraszek, Z. Libohova, J. Benavides-Solorio, and K. Schaffrath (2009), Causes of post-fire runoff and erosion: Water repellency, cover, or soil sealing?, *Soil Sci. Soc. Am. J.*, *73*, 1393–1407.

Lavee, H., P. Kutiel, M. Segev, and Y. Benyamini (1995), Effect of surface roughness on runoff and erosion in a Mediterranean ecosystem: The role of fire, *Geomorphology*, *11*, 227–234.

Lewis, S. A., J. Q. Wu, and P. R. Robichaud (2006), Assessing burn severity and comparing soil-water repellency, Hayman Fire, Colorado, *Hydrol. Processes*, *20*, 1–16.

Liggett, J. E., A. D. Werner, and C. T. Simmons (2012), Influence of the first-order exchange coefficient on simulation of coupled surface–subsurface flow, *J. Hydrol.*, *414*, 503–515.

Loague, K., C. S. Heppner, B. A. Ebel, and J. E. VanderKwaak (2010), The quixotic search for a comprehensive understanding of hydrologic response at the surface: Horton, Dunne, Dunton, and the role of concept-development simulation, *Hydrol. Processes*, *24*(17), 2499–2505.

Loaiciga, H. A., D. Pedreros, and D. Roberts (2001), Wildfire-streamflow interactions in a chaparral watershed, *Adv. Environ. Res.*, *5*, 295–305.

Lucas, J. (2013), September 2013 front range flooding event, *Colo. Water*, *30*(6), 12–17.

Luce, C. H., and T. W. Cundy (1994), Parameter identification for a runoff model for forest roads, *Water Resour. Res.*, *30*(4), 1057–1069, doi:10.1029/93WR03348.

Lyon, S. W., S. L. Desilets, and P. A. Troch (2008), Characterizing the response of a catchment to an extreme rainfall event using hydrometric and isotopic data, *Water Resour. Res.*, *44*, W06413, doi:10.1029/2007WR006259.

MacDonald, L. H., and E. L. Huffman (2004), Post-fire water repellency: Persistence and soil moisture thresholds, *Soil Sci. Soc. Am. J.*, *68*, 1729–1734.

Martin, D. A., and J. A. Moody (2001), Comparison of soil infiltration rates in burned and unburned mountainous watersheds, *Hydrol. Processes*, *15*, 2893–2903.

Martınez-Casasnovas, J. A., M. C. Ramos, and M. Ribes-Dasi (2002), Soil erosion caused by extreme rainfall events: Mapping and quantifica-tion in agricultural plots from very detailed digital elevation models, *Geoderma*, *105*(1), 125–140.

Mataix-Solera, J., V. Arcenegui, N. Tessler, R. Zornoza, L. Wittenberg, C. Martínez, P. Caselles, A. Pérez-Bejarano, D. Malkinson, and M. M. Jordán (2013), Soil properties as key factors controlling water repellency in fire-affected areas: Evidences from burned sites in Spain and Israel, *Catena*, *108*, 6–13.

Maxwell, R. M., and S. J. Kollet (2008), Quantifying the effects of three-dimensional subsurface heterogeneity on Hortonian runoff processes using a coupled numerical, stochastic approach, *Adv. Water Resour.*, *31*, 807–817, doi:10.1016/j.advwatres.2008.01.020.

Meyerhoff, S. B., and R. M. Maxwell (2011), Quantifying the effects of subsurface heterogeneity on hillslope runoff using a stochastic approach, *Hydrogeol. J.*, *19*, 1515–1530.

Mirus, B. B., and K. Loague (2013), How runoff begins (and ends): Characterizing hydrologic response at the catchment scale, *Water Resour. Res.*, *49*, 2987–3006, doi:10.1002/wrcr.20218.

Mirus, B. B., B. A. Ebel, C. S. Heppner, and K. Loague (2011), Assessing the detail needed to capture rainfall-runoff dynamics with physics-based hydrologic response simulation, *Water Resour. Res.*, *47*, W00H10, doi:10.1029/2010WR009906.

Moody, J. A. (2012), An analytical method for predicting postwildfire peak discharges, U.S. Geol. Surv. Sci. Invest. Rep., 2011-5236, 36 pp.

Moody, J. A. (2016), Estimates of peak flood discharge for 21 sites in the Colorado Front Range in response to extreme rainfall in Septem-ber 2013, *U.S. Geol. Surv. Sci. Invest. Rep.*, 2016-5003, 64 pp., doi:10.3133/sir20165003.

Moody, J. A., and B. A. Ebel (2014), Infiltration and runoff generation processes in fire-affected soils, *Hydrol. Processes*, *28*, 3432–3453, doi: 10.1002/hyp.9857.

Moody, J. A. and D. A. Martin (2001a), Post-fire, rainfall intensity-peak discharge relations for three mountainous watersheds in the Western USA, *Hydrol. Processes*, *15*, 2981–2993.

Moody, J. A., and D. A. Martin (2001b), Initial hydrologic and geomorphic response following a wildfire in the Colorado Front Range, *Earth Surf. Processes Landforms*, *26*, 1049–1070.

Moody, J. A., D. A. Kinner, and X. Ubeda (2009), Linking hydraulic properties of fire affected soils to infiltration and water repellency, *J. Hydrol.*, *379*, 291–303.

Moody, J. A., R. A. Shakesby, P. R. Robichaud, S. H. Cannon, and D. A. Martin (2013), Current research issues related to post-wildfire runoff and erosion processes, *Earth Sci. Rev.*, *122*, 10–37.

Moody, J. A., B. A. Ebel, P. Nyman, D. A. Martin, C. Stoof, and R. McKinley (2016), Relations between soil hydraulic properties and burn sever-ity, *Int. J. Wildland Fire*, *25*, 279–293, doi:10.1071/WF14062.

Moré, J. J., and D. C. Sorensen (1983), Computing a trust region step, *SIAM J. Sci. Stat. Comput.*, *3*, 553–572.

Morris, S. E., and T. A. Moses (1987), Forest fire and the natural soil erosion regime in the Colorado Front Range, *Ann. Assoc. Am. Geogr.*, *77*, 245–254.

Mualem, Y. (1976), A new model for predicting the hydraulic conductivity of unsaturated porous media, *Water Resour. Res.*, *12*, 513–522.

Nahar, N., R. S. Govindaraju, C. Corradini, and R. Morbidelli (2004), Role of run-on for describing field-scale infiltration and overland flow over spatially variable soils, *J. Hydrol.*, *286*, 36–51.

Neary, D. G., C. C. Klopatek, L. F. DeBano, and P. F. Ffolliott (1999), Fire effects on belowground sustainability: A review and synthesis, *For. Ecol. Manage.*, *122*, 51–71, doi:10.1016/S0378-1127(99)00032-8.

New, M., M. Todd, M. Hulme, and P. Jones (2001), Precipitation measurements and trends in the twentieth century, *Int. J. Climatol.*, *21*, 1889–1922, doi:10.1002/joc.680.

Nyman, P., G. Sheridan, and P. N. J. Lane (2010), Synergistic effects of water repellency and macropore flow on the hydraulic conductivity of a burned forest soil, south-east Australia, *Hydrol. Processes*, *24*, 2871–2887, doi:10.1002/hyp.7701.n.

Nyman, P., G. J. Sheridan, H. G. Smith, and P. N. Lane (2011), Evidence of debris flow occurrence after wildfire in upland catchments of south-east Australia, *Geomorphology*, *125*(3), 383–401.

Nyman, P., G. J. Sheridan, H. G. Smith, and P. N. Lane (2014), Modeling the effects of surface storage, macropore flow and water repellency on infiltration after wildfire, *J. Hydrol.*, *513*, 301–313.

Ogden, F. L., H. O. Sharif, S. U. S. Senarath, J. A. Smith, M. L. Baeck, and J. R. Richardson (2000), Hydrologic analysis of the Fort Collins, Colo-rado, flash flood of 1997, *J. Hydrol.*, *228*, 82–100.

Onda, Y., W. E. Dietrich, and F. Booker (2008), Evolution of overland flow after a severe forest fire, Point Reyes, California, *Catena*, *72*, 13–20.

Parizek, J. R., and G. H. Girty (2014), Assessing volumetric strains and mass balance relationships resulting from biotite-controlled weather-ing: Implications for the isovolumetric weathering of the Boulder Creek Granodiorite, Boulder County, Colorado, USA, *Catena*, *120*, 29–45.

Perica, S., D. Martin, S. Pavlovic, I. Roy, M. St. Laurent, C. Trypaluk, D. Unruh, M. Yekta, and G. Bonnin (2013), Precipitation-frequency atlas of the United States, Midwestern States, *NOAA Atlas 14*, version 2, vol. 8, NOAA, Natl. Weather Serv., Silver Spring, Md.

Philip, J. R. (1957), The theory of infiltration: 5. The influence of the initial moisture content, *Soil Sci.*, *84*, 329–340.

Prosser, I. P., and L. Williams (1998), The effect of wildfire on runoff and erosion in native Eucalyptus forest, *Hydrol. Processes*, *12*, 251–265.

Ran, Q., C. S. Heppner, J. E. VanderKwaak, and K. Loague (2007), Further testing of the integrated hydrology model (InHM): Multiple-species sediment transport, *Hydrol. Processes*, *21*(11), 1522–1531.

Ran, Q., K. Loague, and J. E. VanderKwaak (2012), Hydrologic-response-driven sediment transport at a regional scale, process-based simula-tion, *Hydrol. Processes*, *26*(2), 159–167.

Reneau, S. L., D. Katzman, G. A. Kuyumjian, A. Lavine, and D. V. Malmon (2007), Sediment delivery after a wildfire, *Geology*, *35*, 151–154.

Rengers, F. K., G. E. Tucker, J. A. Moody, and B. A. Ebel (2016), Illuminating wildfire erosion and deposition patterns with repeat terrestrial lidar, *J. Geophys. Res. Earth Surf.*, *121*, 588–608, doi:10.1002/2015JF003600.

Reynolds, W. D., and D. E. Elrick (2002), Constant head soil core (tank) method, in *Methods of Soil Analysis. Part 4: Physical Methods, Am. Book Ser.*, vol. 5, edited by J. H. Dane and G. C. Topp, pp. 804–808, Soil Sci. Soc. of Am., Madison, Wis.

Reynolds, W. D., and W. D. Zebchuck (1996), Use of contact material in tension infiltrometer measurements, *Soil Technol.*, *9*, 141–159.

Robichaud, P. R. (2000), Fire effects on infiltration rates prescribed fire in Northern Rocky Mountain forests, USA, *J. Hydrol.*, *231–232*, 220–229.

Robichaud, P. R., J. L. Beyers, and D. G. Neary (2000), Evaluating the effectiveness of postfire rehabilitation treatments, *Gen. Tech. Rep. RMRS-GTR-63*, U. S. Dep. of Agric., For. Serv. Rocky Mt. Res. Stn, Fort Collins, Colo.

Rowe, P. B., C. M. Countryman, and H. C. Storey (1954), *Hydrologic Analysis Used to Determine Effects of Fire on Peak Discharge and Erosion Rates in Southern California Watersheds*, USDA For. Serv., Calif. For. and Range Exp. Stn., Berkeley, Calif.

Rulli, M. C., and R. Rosso (2007), Hydrologic response of upland catchments to wildfires, *Adv. Water Resour.*, *30*, 2072–2086.

Saghafian, B., P. Y. Julien, and F. L. Ogden (1995), Similarity in catchment response, *Water Resour. Res.*, *31*, 1533–1541.

Shakesby, R. A., and S. H. Doerr (2006), Wildfire as a hydrological and geomorphological agent, *Earth Sci. Rev.*, *74*, 269–307.

Shakesby, R. A., S. H. Doerr, and R. P. D. Walsh (2000), The erosional impact of soil hydrophobicity: Current problems and future research directions, *J. Hydrol.*, *231*, 178–191.

Sheridan, G. J., P. N. J. Lane, and P. J. Noske (2007), Quantification of hillslope runoff and erosion processes before and after wildfire in a wet Eucalyptus forest, *J. Hydrol.*, *343*, 12–28.

Sherriff, R. L., and T. T. Veblen (2006), Ecological effects of changes in fire regimes in *Pinus ponderosa* ecosystems in the Colorado Front Range, *J. Veg. Sci.*, *17*, 705–718.

Smerdon, B., C. Mendoza, and K. Devito (2007), Simulations of fully coupled lake-groundwater exchange in a subhumid climate with an integrated hydrologic model, *Water Resour. Res.*, *43*, W01416, doi:10.1029/2006WR005137.

Smith, J. A., M. L. Baeck, J. E. Morrison, and P. Sturdevant-Rees (2000), Catastrophic rainfall and flooding in Texas, *J. Hydrometeorol.*, *1*, 5–25.

Smith, J. A., M. L. Baeck, Y. Zhang, and C. A. Doswell III (2001), Extreme rainfall and flooding from supercell thunderstorms, *J. Hydrometeorol.*, *2*, 469–489.

Smith, J. A., G. Villarini, and M. L. Baeck (2011), Mixture distributions and the hydroclimatology of extreme rainfall and flooding in the eastern United States, *J. Hydrometeorol.*, *12*, 294–309.

Smith, R. E. (2002), Infiltration Theory for Hydrologic Applications, *Water Resour. Monogr.*, vol. 15, 212 pp. AGU, Washington, D. C.

Smith, R. E., and D. C. Goodrich (2000), Model for rainfall excess patterns on randomly heterogeneous areas, *J. Hydrol. Eng.*, *5*, 355–362.

Smith, R. E., and R. H. B. Hebbert (1979), A Monte Carlo analysis of the hydrologic effects of spatial variability of infiltration, *Water Resour. Res.*, *15*(2), 419–429.

Smith, R. E., D. C. Goodrich, D. A. Woolhiser, and C. L. Unkrich (1995), KINEROS—A kinematic runoff and erosion model, in *Computer Models of Watershed Hydrology*, edited by V. P. Singh, pp. 697–732, Water Resour. Publ., Highlands Ranch, Colo.

Staley, D. M., T. A. Wasklewicz, and J. W. Kean (2014), Characterizing the primary material sources and dominant erosional processes for post-fire debris-flow initiation in a headwater basin using multi-temporal terrestrial laser scanning data, *Geomorphology*, *214*, 324–338.

Stewart, R. D., D. E. Rupp, M. R. A. Najm, and J. S. Selker (2013), Modeling effect of initial soil moisture on sorptivity and infiltration, *Water Resour. Res.*, *49*, 7037–7047.

Stoof, C. R., J. G. Wesseling, and C. J. Ritsema (2010), Effects of fire and ash on soil water retention, *Geoderma*, *159*, 276–285.

Stoof, C. R., R. W. Vervoort, J. Iwema, E. van den Elsen, A. J. D. Ferreira, and C. J. Ritsema (2012), Hydrological response of a small catchment burned by experimental fire, *Hydrol. Earth Syst. Sci.*, *16*, 267–285, doi:10.5194/hess-16-267-2012.

Stoof, C. R., A. J. D. Ferreira, W. Mol, J. Van den Berg, A. De Kort, S. Drooger, E. C. Slingerland, A. U. Mansholt, C. S. S. Ferreira, and C. J. Ritsema (2015), Soil surface changes increase runoff and erosion risk after a low–moderate severity fire, *Geoderma*, *239*, 58–67.

Tessler, N., L. Wittenberg, and N. Greenbaum (2013), Soil water repellency persistence after recurrent forest fires on Mount Carmel, Israel, *Int. J. Wildland Fire*, *22*(4), 515–526.

Tiedemann, A. R., C. E. Conrad, J. H. Dieterich, J. W. Hornbeck, W. F. Megahan, L. A. Viereck, and D. D. Wade (1979), Effects of fire on water. A state-of-art review, *Gen. Tech. Rep. WO-GTR-10*, vol. 10, U.S. Dep. of Agric., U.S. For. Serv., Denver, Colo.

Tittel, J., O. Büttner, K. Freier, A. Heiser, R. Sudbrack, and G. Ollesch (2013), The age of terrestrial carbon export and rainfall intensity in a temperate river headwater system, *Biogeochemistry*, *115*, 53–63, doi:10.1007/s10533-013-9896-3.

Topp, G. C., and P. A. Ferré (2002), Methods for measurement of soil water content: Thermogravimetric using convective oven-drying, in *Methods of Soil Analysis. Part 4: Physical Methods, Am. Book Ser.*, vol. 5, edited by J. H. Dane and G. C. Topp, pp. 422–424, Soil Sci. Soc. of Am., Madison, Wis.

Turner, M. G. (2010), Disturbance and landscape dynamics in a changing world, *Ecology*, *91*, 2833–2849.

Turner, M. G., W. H. Romme, R. H. Gardner, R. V. O'Neill, and T. K. Kratz (1993), A revised concept of landscape equilibrium: Disturbance and stability on scaled landscapes, *Landscape Ecol.*, *8*, 213–227.

Ubeda, X., S. Bernia, and E. Simelton (2005), The long-term effects on soil properties from a forest fire of varying intensity in a Mediterranean environment, *Dev. Earth Surf. Processes*, *7*, 87–102.

VanderKwaak, J. E. (1999), Numerical simulation of flow and chemical transport in integrated surface-subsurface hydrologic systems, PhD dissertation, 217 pp., Univ. of Waterloo, Waterloo, Ont., Canada.

Vandervaere, J.-P., M. Vauclin, and D. A. Elrick (2000), Transient flow from tension infiltrometers: II. Four methods to determine sorptivity and conductivity, *Soil Sci. Soc. Am. J.*, *64*, 1272–1284.

van Genuchten, M. T. (1980), A closed-form equation for predicting the hydraulic conductivity of unsaturated soils, *Soil Sci. Soc. Am. J.*, *44*(5), 892–898.

van Genuchten, M. T., F. J. Leij, and S. R. Yates (1991), The RETC code for quantifying the hydraulic functions of unsaturated soils, *Rep. EPA/600/2091/065*, Robert S. Kerr Environ. Res. Lab., Off. of Res. and Dev., U.S. Environ. Prot. Agency, Ada, Okla.

Veblen, T. T., K. S. Hadley, E. M. Nel, T. Kitzberger, M. Reid, and R. Villalba (1994), Disturbance regime and disturbance interactions in a Rocky Mountain subalpine forest, *J. Ecol.*, *82*, 125–135.

White, I., and M. J. Sully (1987), Macroscopic and microscopic capillary length and time scales from field infiltration, *Water Resour. Res.*, *23*, 1514–1522.

Wittenberg, L. E. A., and M. Inbar (2009), The role of fire disturbance on runoff and erosion processes—A long-term approach, Mt. Carmel case study, Israel, *Geogr. Res.*, *47*(1), 46–56.

Woods, S. W., A. Birkas, and R. Ahl (2007), Spatial variability of soil hydrophobicity after wildfires in Montana and Colorado, *Geomorphology*, *86*, 465–479.

Yochum, S. E., and D. S. Moore (2013), *Colorado Front Range Flood of 2013: Peak flow estimates at selected mountain stream locations*, 38 pp., U.S. Dep. of Agric., Nat. Resour. Conserv. Serv., Colo. State Off., Fort Collins., doi: 10.13140/2.1.2593.0242

Yochum, S. E., B. P. Bledsoe, G. C. L. David, and E. Wohl (2012), Velocity predictions in high-gradient channels, *J. Hydrol.*, *424–425*, 84–98.